Article

Colours of Gemmy Phosphates from the Gavà Neolithic Mines (Catalonia, Spain): Origin and Archaeological Significance

Yael Díaz-Acha [1,*], Marc Campeny [1], Lluís Casas [2], Roberta Di Febo [3], Jordi Ibañez-Insa [4], Tariq Jawhari [5], Josep Bosch [6], Ferran Borrell [7], Susana Esther Jorge-Villar [8], Jean-Marc Greneche [9], Esperança Tauler [10] and Joan Carles Melgarejo [10]

1   Museu de Ciències Naturals de Barcelona, Parc de la Ciutadella s/n, 08003 Barcelona, Spain; mcampenyc@bcn.cat
2   Departament de Geologia, Universitat Autònoma de Barcelona (UAB), Edifici C, 08193 Cerdanyola del Vallès, Spain; lluis.casas@uab.cat
3   Institut Català d'Arqueologia Clàssica (ICAC), Plaça d'en Rovellat, 43003 Tarragona, Spain; rdifebo@icac.cat
4   Geosciences Barcelona (GEO3BCN), Spanish Council for Scientific Research (CSIC), Lluís Solé i Sabarís s/n, 08028 Barcelona, Spain; jibanez@geo3bcn.csic.es
5   Centres Científics i Tecnològics, Universitat de Barcelona, Lluís Solé i Sabarís, 08028 Barcelona, Spain; jawhari@ccit.ub.edu
6   Museu de Gavà, Plaça de Dolors Clua 13, 08850 Gavà, Spain; jbosch@gava.cat
7   Spanish National Research Council (IMF-CSIC), Egipcíaques 15, 08001 Barcelona, Spain; ferran.borrell@imf.csic.es
8   National Research Center on Human Evolution, CENIEH, 09002 Burgos, Spain; susanajorgevillar@hotmail.com
9   Institut des Molécules et Matériaux du Mans, IMMM UMR CNRS 6283, Le Mans Université, CEDEX 9, 72085 Le Mans, France; jean-marc.greneche@univ-lemans.fr
10 Departament de Mineralogia, Petrologia i Geologia Aplicada, Facultat de Ciències de la Terra, Universitat de Barcelona, Martí i Franquès s/n, 08028 Barcelona, Spain; esperancatauler@ub.edu (E.T.); joan.carles.melgarejo.draper@ub.edu (J.C.M.)
*   Correspondence: ydiaz@bcn.cat; Tel.: +34-93-256-2185

Abstract: In the Neolithic Gavà mines, variscite and turquoise were exploited for ornaments manufacturing, although some prospective pits and tunnels were dug on other similar greenish minerals such as smectite or kandite. A 3D study of the distribution of mineral phases allows us to determine the parameters involved in variscite colours. Methods are comprised of quantitative colourimetry, thin section petrography, SEM-BSE-EDS, EMPA, XRD, Raman spectroscopy, and ^{57}Fe Mössbauer spectrometry. Mapping of the mines indicates that colour is not directly dependent on depth. Although variscite from Gavà is poor in Cr^{3+} and V^{+3} compared with gemmy variscite from other localities, the deep green samples content has the highest values of Cr^{3+}. In the case of cryptocrystalline mixtures with jarosite, phosphosiderite, or goethite, variscite tends to acquire a greenish brown to olivaceous hue. If white minerals such as quartz, kandite, crandallite, or alunite are involved in the mixtures, variscite and turquoise colours become paler.

Keywords: colour; variscite; turquoise; phosphates; neolithic mines; Gavà

1. Introduction

Colour is a very noticeable feature of minerals. Sometimes it can be a powerful diagnostic property but, in other cases, it is very variable and unreliable. There are several causes that control minerals' colouration. Most of them are related to electronic transitions [1], e.g., crystal field transitions within a chromophore element [2] such as Cr, Mn, Fe, Co, Ni, Cu, or V; charge transfer between elements [3,4], and colour centers associated to structural defects [5]. Physical impurities and fine intergrowth structures can also be a source of colour.

Variscite ($AlPO_4 \cdot 2H_2O$) is a common supergene hydrated aluminum phosphate which occurs as phanerocrystalline and cryptocrystalline aggregates. Based on the stoichiometric composition, variscite should be colourless, but this is extremely rare and it generally presents very strong colours. Phanerocrystalline variscite is scarce and tends to occur as a weathering product of Mn-rich evolved granite pegmatites, forming radial aggregates filling cavities or veinlets. This variety presents a typical vitreous lustre with intense emerald green or red colourations. The cause of its colour is attributed to the substitution of Al by Fe^{3+}, Mn^{2+}, or Mn^{3+} [6,7]. Similar red or pinkish aggregates are observed in some occurrences produced by weathering of manganese ores; in such cases, colours are attributed to slight substitutions of Al by Mn^{2+} [8,9]. However, the most striking variety, historically known as calaite, is cryptocrystalline. It presents a waxy lustre and is typically coloured in different shades of green, including apple, brownish, yellowish, or bluish tones, which can remember those of turquoise. This variety of variscite has been used in the manufacturing of ornaments since the Neolithic times in many areas of Western Europe, where corresponding mining sites have been also found. Significant examples of these prehistorical uses of variscite have been reported in northern Portugal [10], France [11], and Spain [12–15]. In fact, variscite was also mined during pre-Hispanic times in South America [16,17] and more recently in North America [18] and Australia [19].

Hence, the study of variscite and its associated mineral phases can provide interdisciplinary information related to the fields of mineralogy, economic geology, and archaeology. In the latter, its characterization and the corresponding study of colours can provide significant data about the source area of archaeological remains and ornaments, among other reasons (e.g., development of exchange networks and construction of cultural identities). Moreover, changes in variscite colour were attributed to the grade of Fe oxidation [20] and could therefore provide information about the level of finding in a single deposit [21]. First works focused on the study of variscite colouration indicated that a typical greenish colour was probably produced by the occurrence of chromophores such as Cr^{3+} [22]. Other authors also pointed out that this colouration could be also generated by the presence of V^{4+} [23,24] or V^{3+} [2,25]. Lately, a systematic study comparing variscite samples from three different European localities concluded that octahedral Cr^{3+} was the probable responsible of the variscite green tone [26].

However, there is some evidence suggesting that the variscite green colour is not only related to the presence of compositional structural impurities (chromophores) but also is associated to crystalline defects. In fact, there exists two different polymorphic types of variscite: the Messbach-type and Lucin-type. The difference between both polytypes is related to the structural position of water molecules: W1 and W2. The W2 molecules are bonded through a single H-bond while W1 is doubly bonded to the lattice through H-bonds. The W1:W2 ratio varies from 1:1 in the Lucin-type to 3:1 in the Messbach-type [27]. Considering the difference between both polytypes, it is well known that variscite can be turned from the Messbach-type to the Lucin-type by continuous exposure to a halogen lamp that simulates sunlight [28]. This polymorphic change also generates a significant loss of colour, suggesting that structural variations can also affect variscite colouration.

The present work is focused on the study of the colour and chemical characterization of the variscite from the Gavà area (Catalonia, NW Spain). In the vicinity of this locality, variscite was exploited during the Neolithic age in a unique and outstanding underground mining complex that was active between 4200 and 3600 cal. BC, and is considered one of the most ancient pieces of evidence of underground mining in Europe [29–41]. It is estimated that several hectares in the Gavà area were affected by mining activity but only a few tens of mines have been totally or partially excavated among the more than 100 shafts or galleries identified in the area [42]. Mining structures vary in complexity and size from short (2–3 m depth), vertical, or sub-vertical shafts, which evolved to complex mining structures reaching a depth of up to 15 m, to chambers and horizontal tunnel-shaped galleries at different levels [20,43–46].

In Gavà, variscite is typically featured by having a wide spectrum of green tones: whitish, olive green, moss green, apple green, or also bluish green. This range of strong colours can be perfectly distinguished by observing fresh geological samples but also in the recovered Neolithic ornaments and jewelry (beads, perforated plaquettes, pendants, and 'medals') found during the archaeological excavations [36,37,40–42,44,47,48]. However, the Gavà variscite is poor in Cr^{3+} and V^{3+} compared to other samples from several European localities such as Pannecé (France) or Palazuelo de las Cuevas, San Vicente, and El Bostal (Zamora, Spain) [49]. Therefore, the real causes of the Gavà variscite colour variation are still underknown. Thus, in the present work, we analyzed and compared geological materials and archaeological samples from the Gavà area to identify the causes of variscite colouration and to go forward in the implications for the study and interpretation of the archaeological remains.

2. Geological Settings

The Gavà municipality is located in the NE sector of the Iberian Peninsula, 20 km SE from the city of Barcelona (Figure 1). The Gavà area is part of the Catalan Coastal Ranges (CCR). The CCR is a NE-SW mountain range flanked by the Ebro Basin to the NW and by the Mediterranean Sea to the SE. It is divided by two parallel mountain systems (Litoral and Prelitoral) separated by the Prelitoral Depression [50,51] (Figure 1). The current relief of the CCR was formed during the Alpine orogeny (late Eocene) but the outcropping materials are part of the Palaeozoic basement that was already deformed and metamorphosed during the Hercynian orogeny [52] (Figure 1). In the CCR, variscite outcrops are common; however, only the Gavà mines are recognized as a source of this material during the Neolithic period [43–45].
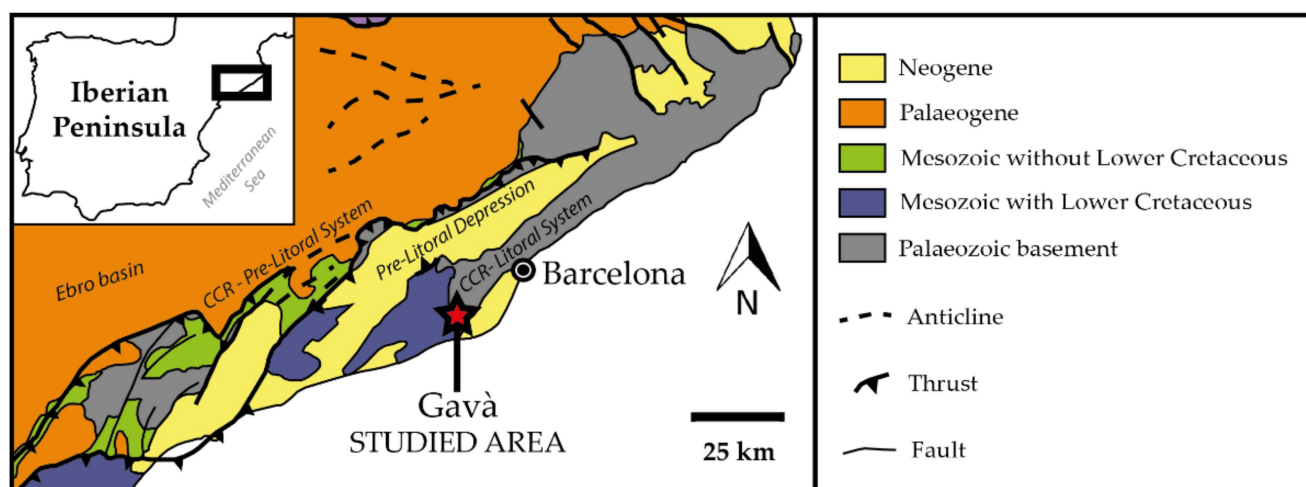
Figure 1. Location map of the study area including the main geological units of the Catalan Coastal Ranges (CCR).

Two main geological units are distinguished in the CCR reliefs: (1) a Paleozoic basement and (2) an unconformably lying Mesozoic sedimentary cover. The basement is made up by metasedimentary series (Cambrian to Mississippian) folded and metamorphosed during the Hercynian orogeny and intruded on by Permian granitoids. The rift basins, as a result of the compressive faulting during the Alpine orogeny, followed by extensional faulting during the Neogene, were filled by syntectonic Neogene sediments [52] (Figure 1).

Gavà lies on the folded and metamorphosed Palaeozoic basement, covered at the NW by unconformable Mesozoic sediments. This set of materials, in turn, is unconformably covered by Quaternary calcrete and reddish clays with carbonate nodules up to 3 m thick [43,53].

Supergene mineralization is only hosted in the Silurian series of the Paleozoic basement. These correspond to sulphide-rich black shales of Llandoverian age and interbedded with layers of a few centimeter-thick and nodules of fluorapatite and chert [20,43–46,54]. These rocks are pale grayish in the surface outcrop and, below the Quaternary unconformity, they become progressively darker downwards, reaching the original black colour at a depth of 15 m. The variation in colour of the shales has been attributed to the oxidation of the contained organic matter during the interaction with oxidizing acid fluids. This process, linked to weathering processes, was produced by sulphides' leaching during the early Pleistocene. These acid solutions also leached phosphate from the apatite beds and altered the illite from the shales, which explains the occurrence of aluminophosphates. Phosphates occur as veinlets (1 mm to 4 cm in width) or replace the sedimentary apatite nodules and beds. Supergenic phosphates (e.g., variscite, montgomeryite, crandallite, and phosphosiderite) occur along with sulphates (e.g., jarosite and alunite); they are also associated with quartz and clay minerals (e.g., halloysite and smectite) [20].

3. Study Area

The variscite mineralization found in the Gavà area is generally revealed by Neolithic mining galleries [20,43–46]. To date, more than 100 Neolithic mines have been reported in the area and they are especially concentrated in two different sectors: Can Tintorer and Les Ferreres (Figure 2).

3.1. Can Tintorer Sector

The Can Tintorer sector is located at the north of the Gavà downtown (Figure 2). Until the mid-20th century, the area was not urbanized, but, nowadays, this sector is densely built up. Therefore, the labors of several Neolithic mines were buried under recent sediments and covered by modern constructions. Even so, the major number of excavated prehistorical mines (about 75) in this sector has currently been reported. The most important cluster of galleries is reasonably preserved and it has become an on-site museum: the Gavà Mines Archaeological Park (GMAP). In fact, 190 samples used in the present study were obtained from the GMAP site (Figure 2).

The GMAP consists of eight mines that can be grouped into three different areas: mines 107, 108, and 110 are located at the NE of the complex; mine 16 to the SE; and the largest mine structure, formed by mines 3, 5, 7, and 11, is located in the south (Figure 2b). This last group of mines has an approximate area of 65 m × 30 m and reached up to 15 m in depth [20,45,46].

Mine 16, which reached a depth of 9 m, has a semi-vertical entrance shaft and has been interpreted as a medium-to-large sized complex mining structure [42]. The shaft was filled with anthropogenic deposits, which included archaeological artefacts such as fragments of variscite beads. The most remarkable finding in this mine was an anthropomorphic-figure vessel known as the Venus of Gavà [37,40].

3.2. Les Ferreres Sector

Les Ferreres is located close to west side of the Can Tintorer sector (Figure 2). It is formed by smooth positive reliefs known as the Les Ferreres Range (200 m high).

Mine 85 was discovered and excavated during the year 2000 [55] when two semi-vertical shafts were dug. In the upper shaft, abundant variscite manufactured items (beads, perforated plaquettes, pendants, and 'medals'), among other archaeological materials, were found [42].

Recently, between 2020 and 2021, two new archaeological exploration campaigns were carried out focused on a new archaeological study area next to where the previous mines had been located and it was preliminarily termed for this study as ASA (Figure 2a). Likewise, the area was geologically sampled and mapped, and one of these newly found samples was also used for the present study.
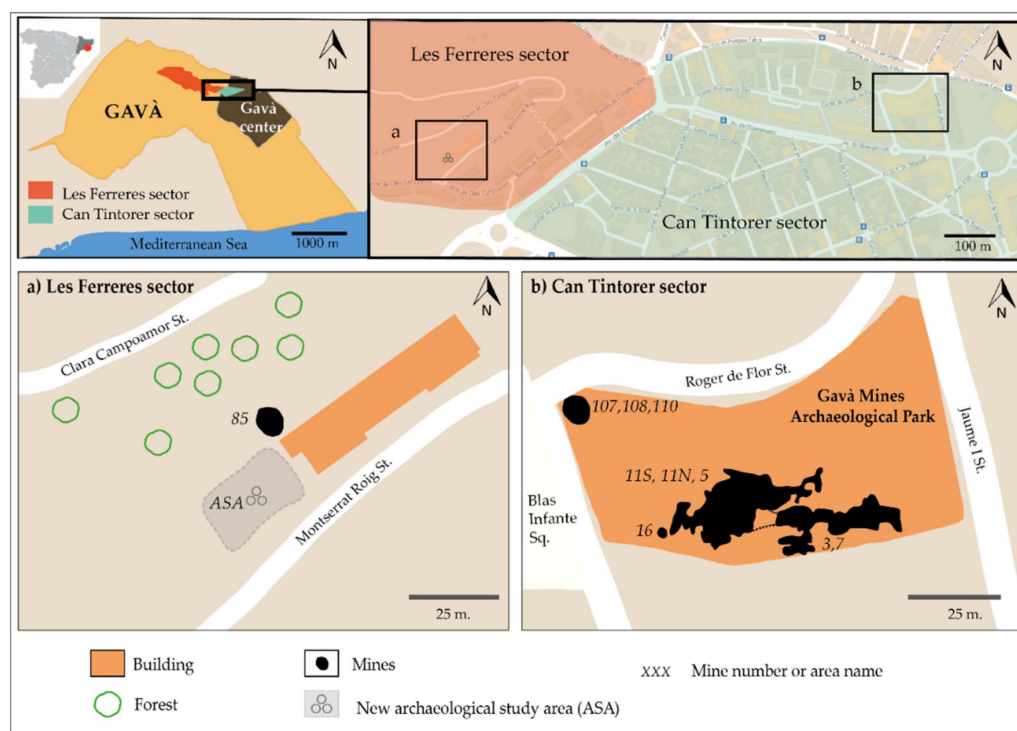
Figure 2. Geographical map of the Gavà area and location of the studied mines in the sectors of Les Ferreres and Can Tintorer. (**a**) Location of mine 85 and the new archaeological study area (ASA) in Les Ferreres sector. (**b**) Location of mines 3, 5, 7, 11, 16, 107, 108, and 110 included in the Gavà Mines Archaeological Park (GMAP).

4. Materials and Methods

4.1. Samples

Fresh variscite samples were obtained from the walls of excavated Neolithic mines. We also studied archaeological items made of variscite found during archaeological works. Geological and archaeological studied materials are representative of both the Gavà studied sectors: Can Tintorer and Les Ferreres.

4.1.1. Mineral Samples

Two geological sampling campaigns were carried out in the Gavà Mines Archaeological Park between 2017 and 2020. The sampling was mainly focused on phosphates and sulphates but with emphasis on the collection of green minerals. Nearly 200 samples were obtained as a result of these campaigns carried out in mines 3, 5, 7, 11, 16, 107, 108, and 110 (Figure 3a). All samples were collected following extensive and representative sampling criteria in depth, from the top of the mines (beginning of the bleached black shales) to the base of the mines, and focusing on supergene mineralization.

In addition, in the framework of a new research project, a large green phosphate nodule was found during the archaeological exploration campaign carried out between 2020 and 2021 in the ASA area from the Les Ferreres sector. This unique and outstanding sample was also analyzed and used in the present work (Figure 3b).

Figure 3. Details of 7 samples (acronym: Gavà Mines (GM); mine name; and sample number) representative of the different colours of variscite from the Gavà mining area. (**a**) Archaeological studied area in Les Ferreres sector, as exposed during the sampling period, with mine entrances (yellow contours) infilled by sediments. The large green nodule (GM-ASA-1) was found cropping on the surface. (**b**) General view of GMAP mines in Can Tintorer sector (by Benet Solina) and corresponding mineral samples showing the diversity of variscite colouration.

4.1.2. Archaeological Samples

Different types of archaeological materials from the Gavà area were studied for comparison with the geological samples. They were comprised of 16 Neolithic ornamental elements (11 from mine 16 and 5 from mine 85; Figure 2) made of variscite such as round and discoidal necklace beads, as well as perforated and unperforated circular or rectangular plates and fragmented plates [38,39,55] (Figure 4). All of these samples were gently provided by the GMAP.
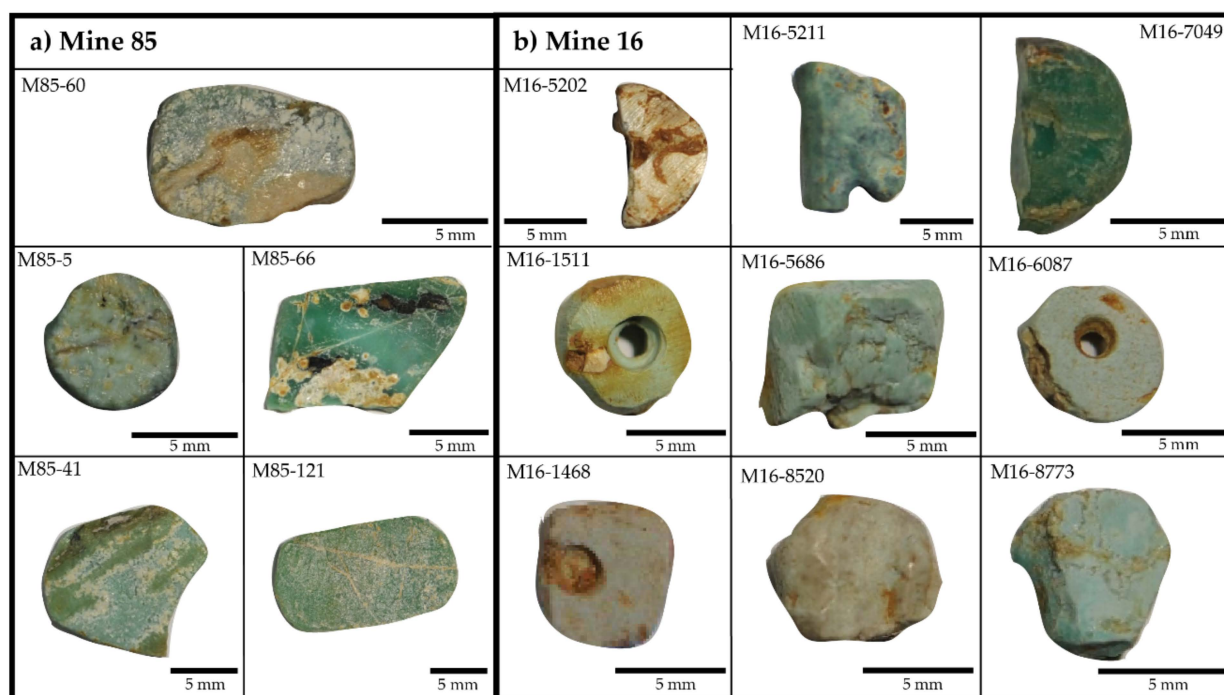
Figure 4. Detailed pictures of the studied archaeological elements. (**a**) Five studied representative items from mine 85 located in Les Ferreres sector. (**b**) Nine from the 11 archaeological items studied from mine 16, which is located in the area of the GMAP.

4.2. Analytical Methods

4.2.1. Colourimetry

In order to determine and classify the colouration of geological and archaeological materials, we carried out colourimetry measurements. The quantitative colour of 16 archaeological items and 12 geological samples was determined using a RM200QC portable spectrocolourimeter (X-rite Inc., Grand Rapids, MI, USA). The measurements were taken on dry samples, selecting the most regular and representative surface as possible. The reproducibility and homogeneity of the measurements were checked by repeating all measurements at least twice and measuring different spots on the samples. The diameter of the measured circular areas was usually set at a 4 mm diameter to avoid surface irregularities and non-representative small veins. Occasionally, for large and homogeneously coloured samples, measurements covering 8 mm diameter circular areas were taken.

The measured colours were obtained as Natural Colour System (NCS) codes and they were transformed into colour Hex values as well as RBG triplets for analyses and representation purposes. The RGB colour space expresses colours with RGB triplets indicating the combination of red (R), green (G), and blue (B) to produce a given colour. The component values usually ranged from 0 to 255. As RGB is an additive colour model, white was represented by (255, 255, 255) and black by (0, 0, 0).

4.2.2. X-ray Diffraction (XRD)

The Gavà supergene mineralization is mostly composed of cryptocrystalline minerals. Hence, variscite and its associated mineral phases were identified by means of X-ray diffraction (XRD).

Archaeological samples have a significant heritage relevance and neither the materials could be destroyed, nor any piece could be disintegrated. Therefore, it was decided to carry out non-destructive in situ powder XRD measurements on these samples, taking advantage of the fact that most of the studied artefacts displayed a nearly flat surface. Thus, conventional Bragg–Brentano XRD analyses were performed directly on the archaeological artefacts by selecting an as-flat-as-possible surface of the samples. With this configuration,

the X-ray beam was larger than the sample surface and therefore some peak broadening may have occurred due to sample roughness and slight sample misalignment. In any case, these experiments still allow one to obtain reliable mineralogical information in a fast and non-destructive manner without any sample preparation. These measurements were carried out at Geosciences Barcelona (GEO3BCN-CSIC, Barcelona, Spain) by using a Bruker D8-A25 diffractometer (CuKα radiation, λ = 1.5406 Å, at 40 kV and 40 mA) equipped with TWIN-TWIN optics; a Lynxeye linear position sensitive detector (PSD); Soller slits; and a Ni filter to remove CuKβ radiation. The XRD scans were collected with 4° to 65° scans (2θ), with an equivalent integration time of 192 s, step size of 0.035° (2θ), and fixed divergence slit. Phase identification was performed by using the software DIFFRAC.EVA in combination with the Powder Diffraction File (PDF-2) and the Crystallography Open Database (COD).

On the other hand, 174 mineral samples obtained from geological outcrops from the GMAP were ground in an agate mortar to produce homogenized powder and randomly oriented material with a particle size below 40 μm. The XRD powder analyses were performed using a PANalytical X'Pert PRO Alpha1 diffractometer at the Scientific and Technological Centres of the University of Barcelona (CCiT-UB, Barcelona, Spain). The diffractometer used a copper anode Cu Kα1 radiation (λ = 1.54056 Å, 45 kV, and 40 mA) and was equipped with a position sensitive detector (PSD) with an amplitude of 2.113°. Diffractograms were obtained by scanning samples from 4° to 80° (2θ) with a scan time of 50 s, step size of 0.017° (2θ), and variable divergence slit. Mineral identification and semi-quantitative results were obtained using the X'Pert HighScore search–match software with Powder Diffraction File 2.0 from ICDD (International Centre for Diffraction Data).

4.2.3. Scanning Electron Microscopy (SEM)

In total, 23 representative samples of variscite and its associated minerals were prepared as polished thin sections for their study under a petrographic microscope at the Laboratory of Geological and Paleontological Preparation (LPGiP) of the Natural Sciences Museum of Barcelona (Barcelona, Spain). Seven selected sections were examined in an environmental scanning electron microscope (SEM), Quanta 200 FEI, XTE 32/D8395, equipped with an energy-dispersive spectrometer (EDS) at the Scientific and Technological Centres of the University of Barcelona (CCiT-UB). Operating conditions were 15–20 kV accelerating voltage and 5 nA beam current.

4.2.4. Electron Probe Microanalysis (EPMA)

A set of 164 fragments of variscite samples and associated minerals were included in epoxy; eight mounts were polished with diamond powder. Quantitative compositional features of such polished mineral surfaces were obtained by means of electron probe microanalyses (EPMA) performed on a JEOL JXA-8230 electron microprobe with five wavelength-dispersive spectrometers (WDS), an energy dispersive spectrometer (EDS), and a silicon-drift EDS detector at the CCiT-UB (Barcelona, Spain).

Spot analyses were carried out with a 15 kV accelerating voltage, a 10 nA beam current, and a focused beam in order to achieve the best lateral resolution. Counting times ranged from 20 to 40 s for both peaks and background. Analytical standards included natural and synthetic silicates, as well as oxides and REE glasses as follows: diopside (Ca *K*α and Si *K*α), spinel (Al *K*α), RbTiOPO$_4$ (P *K*α), periclase (Mg *K*α), hematite (Fe *K*α), orthoclase (K *K*α), and celestite (S *L*α). The correction procedure XPP was used to convert specimen intensity ratios into concentrations. Structural formulae were calculated by assuming Fe$_{total}$ as Fe^{3+} and 4 oxygens for variscite.

4.2.5. Raman Spectroscopy

Raman spectra in archaeological samples were obtained with the dispersive spectrometer Jobin-Yvon LabRam HR 800 coupled to the optical microscope Olympus BXFM with

an excitation laser source emitting at 532 nm at the CCiT-UB (Barcelona, Spain). The laser power at the sample was 5 mW and the used microscope objectives were 100× and 50×.

Mineral samples were analyzed with other Raman spectra carried out in the Archaeometry Laboratory of CENIEH (Spain). A DXR Thermo Fisher confocal Raman spectrometer was used working with a 532 nm laser wavelength (green light). For improving the spectral signal-to-noise ratio, 60 accumulations at a 10-s exposure time were performed at each sampling position. A set of Raman spectra were compiled with laser powers at the sample of 0.1, 0.5, and 1 and 2 mW, and, finally, an operating laser power of 1 mW was selected.

4.3. ^{57}Fe Mössbauer Spectrometry

Three samples identified as variscite and containing significant amounts of Fe were selected for Mössbauer analyses. The Mössbauer samples consisted of a layer of powder containing about 5 mg Fe/cm^2, at least avoiding thickness effects. Spectra were recorded at room temperature (RT) and low temperature (LT, 77 K) in a transmission geometry using a ^{57}Co/Rh γ-ray source mounted on a conventional constant acceleration vibrating electromagnetic transducer (triangular velocity-form). Natural iron foil was used as a standard for velocity calibration. The experimental data were analyzed by a least-square fitting method (unpublished MOSFIT program J. Teillet, F. Varret Université Le Mans France) to Lorentzian functions and the isomer shift values (δ) are referred to as α-Fe at RT.
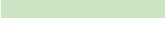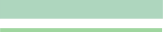
5. Results

5.1. Colourimetry

Colourimetry results expressed as RGB triplets indicate a roughly positive correlation between all three colour channel values. In particular, the correlation coefficient between the blue and green values seemed to be the highest (Figure 5). In the samples with a predomination of the red channel, the colour was perceived as brownish and also usually presented low RGB values. In contrast, samples with higher RGB values tended to present a higher G value than R and B, and, therefore, they were perceived as greenish. In addition, it is worth mentioning that among the archaeological samples, the frequency of brownish colours was lower and generally prevailed as greenish (sometimes even bluish; Table 1).
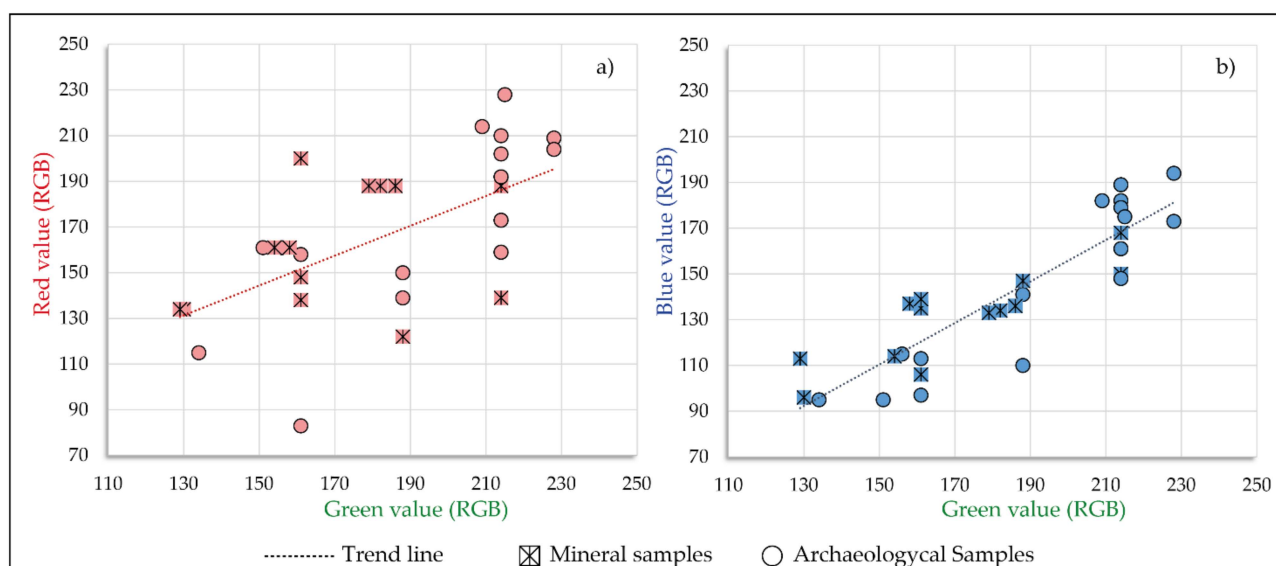
Figure 5. Representation of colourimetry results through the relation between (**a**) red value and green value, and (**b**) blue value and green value. Mineral samples are represented with an asterisk and archaeological samples with circles.

Table 1. Colourimetry results expressed in NCS colour and Hex colour, and the corresponding colour representation for the studied archaeological and mineral samples.

Archaeological Samples				Mineral Samples			
Number	NCS Colour	Hex Colour	Colour	Sample	NCS Colour	Hex Colour	Colour
M16-1468	S2010-Y	#d6d1b6		GM-7-3.3	S3020-Y	#bcb385	
M16-1511	S2020-G40Y	#c0d694		GM-7-3.7	S4010-G30Y	#94a187	
M16-5202	S1515-Y10R	#e4d7af		GM-7-3.9	S4020-Y	#a19a72	
M16-5211	S3020-G10Y	#8bbc8d		GM-7-4.5	S3020-G80Y	#bcba88	
M16-5868	S2020-B90G	#9fd6a1		GM-5/7-3.1	S2020-G50Y	#c8d696	
M16-6087	S1510-G20Y	#cce4c2		GM-5/11-2A.2	S5020-G90Y	#868260	
M16-7044	S4020-G90Y	#a19c73		GM-11N-5.2	S3020-G90Y	#bcb686	
M16-7049	S4020-G10Y	#cad6b3		GM-11N-7.2	S5010-Y10R	#868171	
M16-8520	S2010-G60Y	#d2d6b6		GM-11S-5.1	S3020-G	#7abc93	
M16-8669	S2010-G	#add6bd		GM-11S/3-4,5.2	S4010-G90	#a19e89	
M16-8773	S2010-G	#add6bd		GM-11N-4	S4030-G10Y	#67a16a	
M85-5	S2020-G10Y	#9fd6a1		GM-ASA-1	S2020-G	#8bd6a8	
M85-41	S3030-G30Y	#96bc6e					
M85-60	S2010-G20Y	#c0d6b7					
M85-66	S4030-G	#53a171					
M85-121	S5020-G30Y	#73865f					

5.2. X-ray Diffraction (XRD)

According to the XRD analysis, most of the geological greenish samples from the mines as well as the archaeological greenish ornaments corresponded to cryptocrystalline variscite. Poorly coloured samples contained different proportions of crandallite ($CaAl_3(PO_4)(PO_3OH)(OH)_6$), jarosite ($KFe^{3+}_3(SO_4)_2(OH)_6$), phosphosiderite ($FePO_4 \cdot 2H_2O$), alunite $KAl_3(SO_4)_2(OH)_6$, goethite ($\alpha\text{-}Fe^{3+}O(OH)$), and quartz ($SiO_2$); in addition, clay minerals such as kaolinite ($Al_2Si_2O_5(OH)_4$), halloysite ($Al_2Si_2O_5(OH)_4$), endellite (halloysite-10Å; $Al_2Si_2O_5(OH)_4 \cdot 2H_2O$), and smectite ($A_{0.3}D_{2-3}[T_4O_{10}]Z_2 \cdot nH_2O$) were relatively abundant and had greenish hues in many cases (Figure 6).

Similar results were found in the case of greenish archaeological samples. However, although variscite also predominates among them, turquoise ($CuAl_6(PO_4)_4(OH)_8 \cdot 4H_2O$) can be the main constituent of some pieces from the Can Tintorer sector. In addition, most of the archaeological items were composed, as in the geological samples, by mixtures of the variscite or turquoise minerals with different proportions of phosphosiderite, crandallite, or halloysite. The colours of both turquoise and variscite ranged between grass green to bluish green, whereas minerals of compositions between strengite and Fe-rich variscite ranged from pale brownish (such as jarosite) to olivaceous (such as halloysite). However, veins composed by alunite, crandallite, calcite, quartz, and kaolinite presented white colouration. Finally, veins containing goethite were brownish. These results are similar to those obtained in previous works using thin-section petrography and SEM-BSE-EDS (for instance, see [20]).
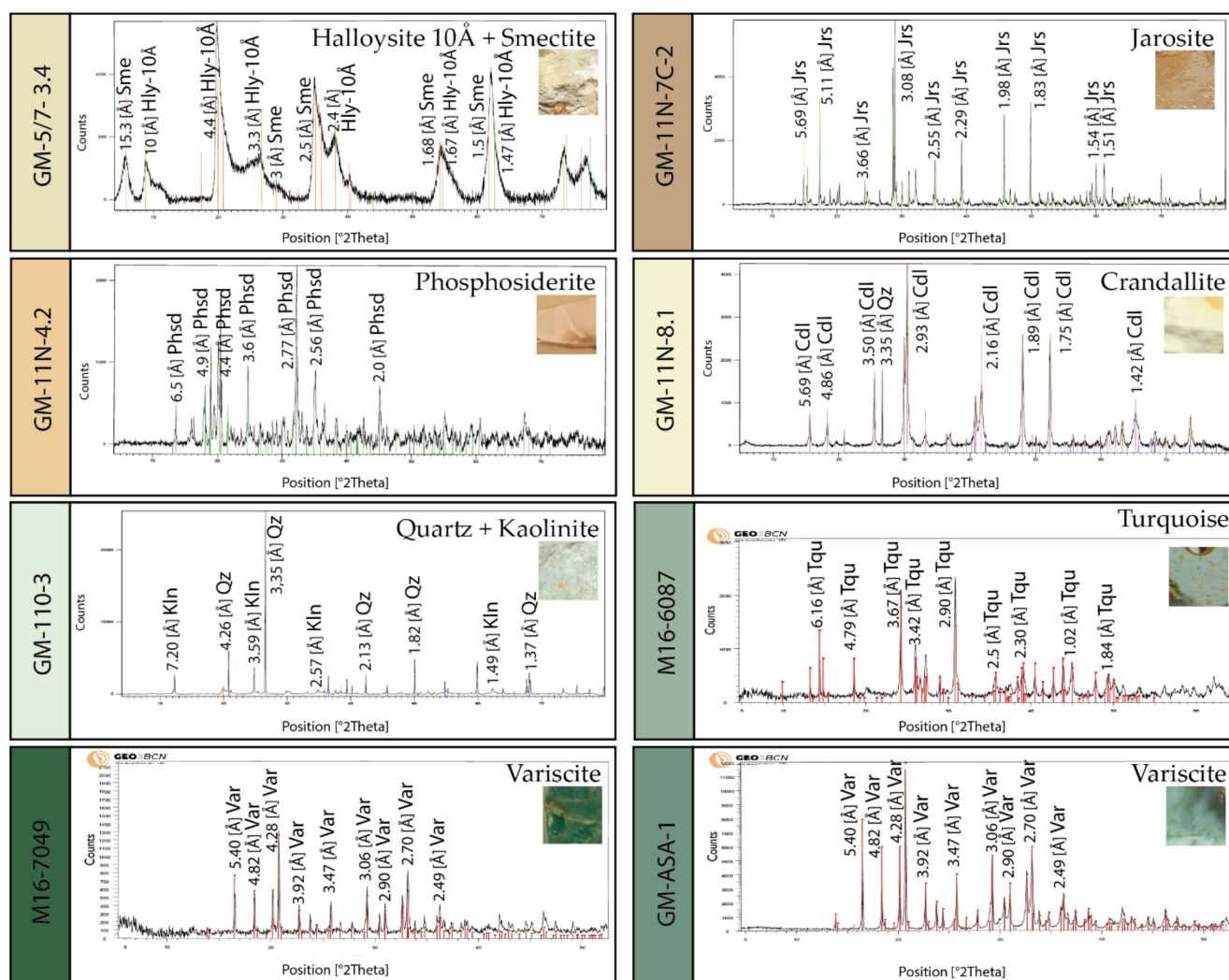
Figure 6. Selected X-ray powder diffractograms representative of different minerals in the Gavà area with different colours. The most characteristic reflections of the dominant minerals have been indicated. Legend: Hly-10Å, halloysite 10Å; Sme, smectite; Kln, kaolinite; Phsd, phosphosiderite; Var, variscite; Tqu, turquoise; Cdl, crandallite; Jrs, jarosite; and Qz, quartz.

5.3. Scanning Electron Microscopy (SEM)

BSE-based SEM images revealed that the Gavà samples consist of cryptocrystalline aggregates since most of the grain sizes were well below 1 micron in diameter. In detail, the veinlets mined in Gavà can present a simple internal texture, being made up by monomineralic homogeneous aggregates and sometimes crosscut by late veinlets of other minerals (Figure 7a). However, most of the veinlets tended to present complex internal structures. A typical texture consists of intimate mixtures of different cryptocrystalline minerals with an irregular distribution, replaced by successive pulses of other cryptocrystalline mixed minerals (Figure 7b,c). Replacement is progressive and irregular, moving from the contact veins/host rock towards the core of the veins (Figure 7c).
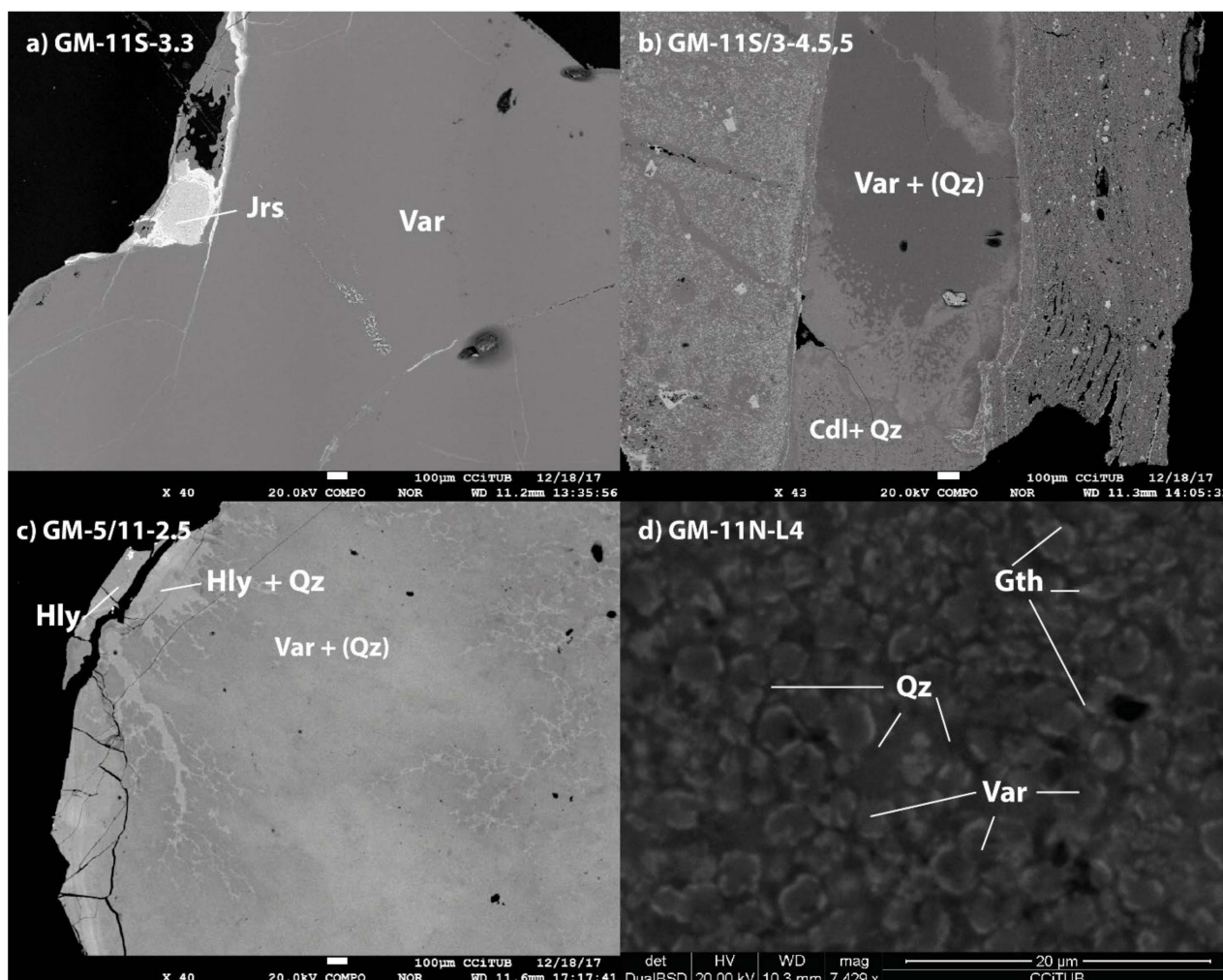
Figure 7. SEM (backscattered electron, BSE) images of different greenish samples from the Gavà area. (**a**) Homogeneous cryptocrystalline variscite (Var) veined and replaced by jarosite (Jrs); brighter veins are made up by goethite. (**b**) Veinlet with mixtures of variscite (Var) with lower proportions of quartz (Qz) is replaced by a mixture of crandallite (Cdl) with quartz (Qz). (**c**) Massive aggregates of cryptocrystalline mixtures of variscite (Var) with minor quartz (Qz) are replaced by mixtures of halloysite (Hly) and quartz (Qz); halloysite becomes dominant at the vein contact with the host rock (which is at the origin at the left of the image). (**d**) Goethite platelets (Gth) found at the contact between variscite nodules (Var) and quartz (Qz).

When examined with a higher magnification, fine-grained mixtures were also recognized in many of the apparently homogeneous units. For instance, one of the most green-coloured studied samples was made up of cryptocrystalline variscite nodules in a cryptocrystalline silica groundmass; tiny goethite platelets occurred at the contact between both minerals (Figure 7d).

5.4. Electron Probe Microanalysis (EPMA)

The obtention of accurate microanalyses of the Gavà minerals is very difficult considering the cryptocrystalline nature of these phases. In addition, mineral aggregates are generally porous and present intimate mixtures with other phases. Low values of the total weight percentage wt.% (also when including the calculated water) are a consequence of the cryptocrystalline and porous texture of these aggregates.

Moreover, the excitation volume of the electronic beam was larger than the grain size of the analyzed minerals. Therefore, variations in the proportions of many components of the variscite analysis can be partially attributed to mixtures with the surrounding minerals.

The most remarkable variations of variscite occurred in their Fe_2O_3 contents, which ranged between 0.5 and 6 wt.%. A variable SiO_2 content may occasionally be present., however, SEM-BSE images combined with XRD results suggest that these variations can be produced by mixtures of quartz, kaolinite, halloysite, or different proportions of other silicates (Figure 8).
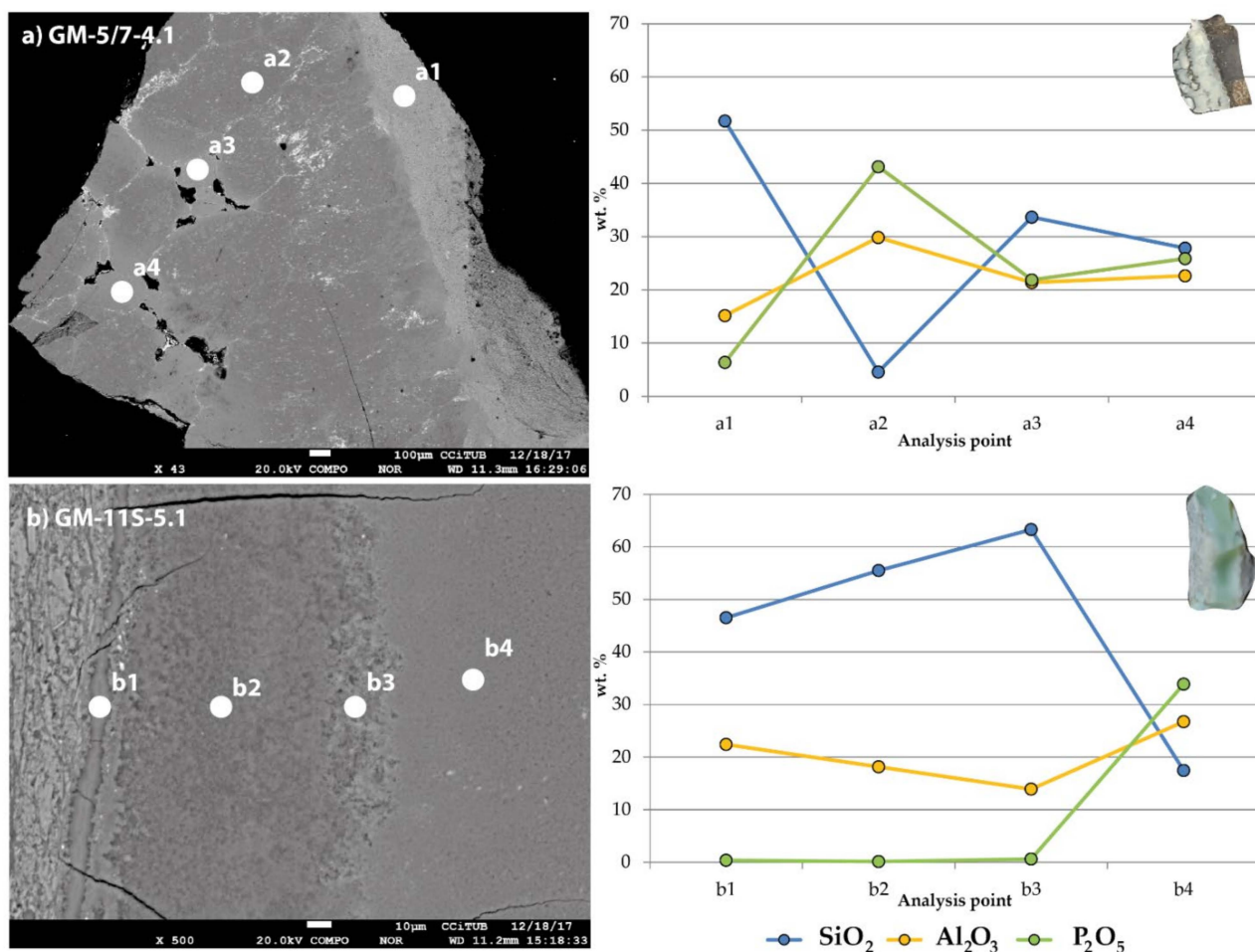
Figure 8. SEM (backscattered electron, BSE) images with labelled EPMA analyses. (**a**) Complex variscite vein (contact with the hosting shale is at the right side of the image) with a first band composed by mixtures of kaolinite and quartz. The innermost part of the vein consists of mixtures of variscite with lower proportions of quartz and is cross-cut by veinlets made up by mixtures of variscite and quartz. The composition of the different analyzed points is not stoichiometric and corresponds to mixtures of different proportions of quartz, kandite, and variscite. (**b**) Banded unit in which it is possible to distinguish in the detail the mixtures of different mineral phases. The darkest part is made up by mixtures of quartz and kaolinite; the brightest, at the right, is composed by quartz and variscite cryptocrystalline mixtures. P_2O_5 values are absent in the three first points. The obtained compositions never correspond to stoichiometric compositions and they are produced by mixtures of quartz and kaolinite in the three first points as well as by mixtures of quartz and variscite in the last one.

However, the most interesting results of the microprobe analyses are those related to minor (trace) elements. The Cr_2O_3 values are in the trace level while most of them below the microprobe detection limit and the highest values achieve 0.17 wt.% (Table 2a,b). Similar low values were detected in the case of V_2O_3, reaching up to 0.14 wt.%.

Phosphosiderite can be enriched in CaO (up to 10 wt.%) and Al_2O_3 (up to 8 wt.%); crandallite can also be enriched in Fe_2O_3 (up to 2 wt.%; Table 2). Rare Earth Elements (REE) were not detected with EDS nor EMPA.

Sheet silicates were strongly enriched in Fe_2O_3 (up to 10 wt.%) and CaO (up to 1.4 wt.%) in practically all the analyzed points (Table 2).

It should be noted that among all the GMAP samples collected and analyzed for the present work, none of them allowed us to detect the presence of turquoise.

5.5. Raman Spectroscopy

Raman analyses were carried out in all the selected archaeological samples. Raman scattering measurements only yielded acceptable results in four samples while the rest showed strong fluorescence signals, giving rise to inconclusive spectra. The resulting spectra confirmed the occurrence of variscite in all four cases; metavariscite was found as a minor component, as revealed by the distinctive peak near 400 cm^{-1} (i.e., [56,57]). The 1028 cm^{-1} peak of the non-oriented variscite (532 nm) was slightly displaced across the profiles in respect to the standard (Figure 9). Similar results were obtained for mineral samples.
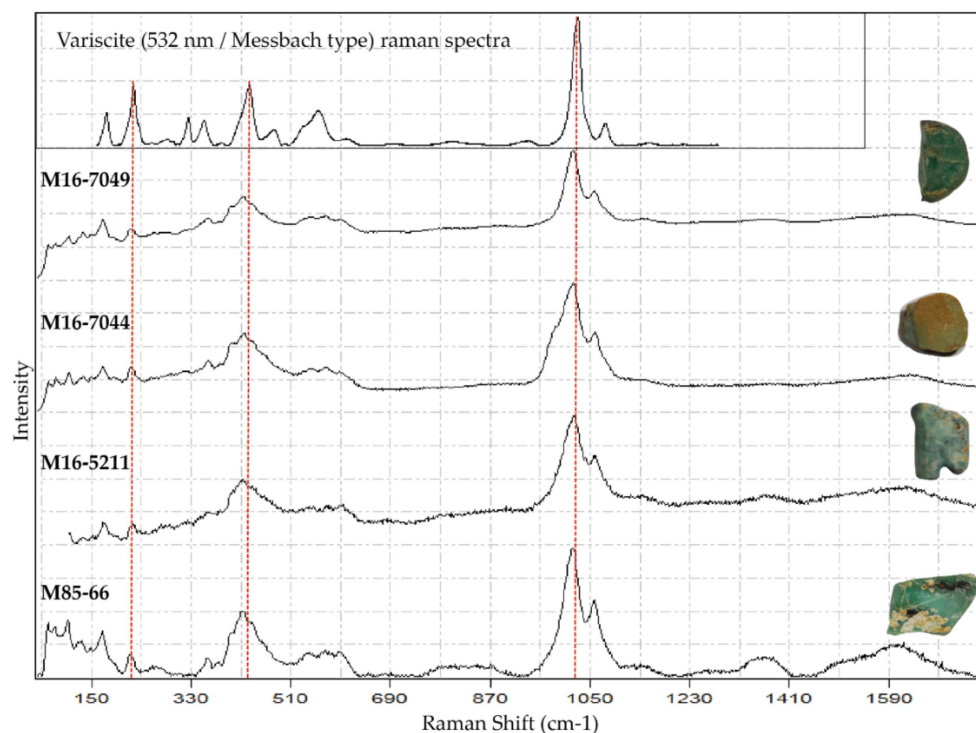
Figure 9. Messbach-type variscite standard of the RRUFF database (top of image; 532 nm laser excitation) compared with the profiles of four archaeological variscite samples from Gavà. Note that poorly defined bands nearby to 400 cm^{-1} are indicative of minor metavariscite occurrences.

Table 2. Electron probe microanalyses (EPMA) in greenish and brownish minerals (geological samples from Can Tintorer).

	(a) Representative Composition of Variscite (Including Cr and V Results).													
Mineral	**Variscite**													
Analysis Number	3-n	5/11-2A2	11S-3.4	11S-3.3	7-3.1	7-3.3	7-3.7	7-3.8	7-4.5	11/3-4.5	5/7-5.1	11N-5.1	11N-6.2	11N-7.2
wt.%														
SiO_2	1.75	0.15	0.62	0.19	2.87	4.08	3.60	2.10	1.69	2.29	0.13	2.45	2.41	4.95
Al_2O_3	29.6	28.9	28.4	29.0	29.5	28.6	29.2	27.0	27.3	28.5	29.1	29.9	29.6	28.6
FeO	2.79	3.05	2.82	2.51	1.91	2.59	1.28	1.74	4.12	1.82	2.63	1.47	3.71	3.23
Fe_2O_3 calculated	3.10	3.39	3.13	2.79	2.12	2.88	1.42	1.93	4.58	0.46	2.92	1.63	4.12	3.59
MgO	bdl	bdl	bdl	bdl	bdl	0.07	bdl	bdl	0.05	0.11	bdl	0.12	bdl	0.04
CaO	0.28	0.21	0.36	0.06	0.67	1.29	1.04	0.68	0.35	0.39	0.16	2.31	0.50	3.62
K_2O	0.04	0.02	0.04	0.03	0.02	0.04	0.03	0.02	0.07	0.27	0.01	0.07	0.03	0.06
P_2O_5	45.0	44.7	44.6	45.0	43.7	41.2	43.0	41.5	44.1	44.2	46.1	41.0	44.2	39.2
SO_3	0.03	0.02	0.14	0.08	0.06	0.11	0.06	1.80	0.08	0.13	0.08	0.16	0.07	0.12
V_2O_3	0.23	bdl	0.08	0.02	0.07	0.03	0.07	0.04	0.11	0.15	0.05	0.06	0.05	0.05
Cr_2O_3	0.05	0.08	0.06	0.07	0.05	0.07	0.04	0.07	bdl	0.04	0.14	0.17	0.07	0.07
Total	79.5	77.1	77.1	76.8	78.7	78.0	78.1	73.1	77.6	77.7	78.1	77.3	80.5	79.7
apfu														
Si	0.045	0.004	0.017	0.005	0.075	0.108	0.094	0.057	0.045	0.060	0.004	0.066	0.062	0.131
Al	0.899	0.909	0.889	0.910	0.905	0.893	0.902	0.867	0.853	0.885	0.897	0.943	0.893	0.887
Fe^{3+}	0.060	0.068	0.063	0.056	0.042	0.057	0.028	0.040	0.091	0.040	0.058	0.033	0.079	0.071
Mg	0.002	0.002	0.002	0.002	0.002	0.002	0.002	0.002	0.002	0.002	0.002	0.005	0.002	0.001
Ca	0.008	0.006	0.010	0.002	0.019	0.037	0.029	0.020	0.010	0.011	0.004	0.066	0.014	0.102
K	0.001	0.001	0.001	0.001	0.001	0.001	0.001	0.001	0.002	0.009	0.000	0.003	0.001	0.002
P	0.983	1.008	1.005	1.014	0.963	0.924	0.953	0.957	0.990	0.985	1.020	0.929	0.960	0.876
S	0.001	0.000	0.003	0.002	0.001	0.002	0.001	0.037	0.002	0.003	0.002	0.003	0.001	0.002
V	0.005	0.000	0.002	0.001	0.001	0.001	0.001	0.001	0.002	0.003	0.001	0.001	0.001	0.001
Cr	0.001	0.002	0.001	0.001	0.001	0.002	0.001	0.001	0.000	0.001	0.003	0.004	0.001	0.001
Total cations	2.001	1.996	1.995	1.989	2.006	2.027	2.009	1.980	1.996	1.998	1.986	2.048	2.010	2.073
Oxygens	4	4	4	4	4	4	4	4	4	4	4	4	4	4

Table 2. *Cont.*

|	(b) Representative Composition of Crandallite, Phosphosiderite, Halloysite, and Jarosite.												
Mineral	Crandallite		Phosphosiderite				Halloysite				Jarosite		
Analysis Number	11S-3.4	11N-7.2	108-5	7-4.7	11N-4.2	11N-7C.2	11N-1.4	7-2.2	5/11-3.6	5/11-5.1	11S-3.1	11S-3.3	7-4.9
wt.%													
SiO_2	5.20	4.52	3.18	6.89	2.18	3.98	51.1	51.9	51.5	51.8	0.02	1.26	0.08
Al_2O_3	29.0	29.8	4.34	8.08	6.06	0.99	34.3	26.4	31.0	26.3	1.09	6.19	0.55
FeO	2.36	1.74	30.5	24.5	33.7	32.1	4.68	9.16	5.98	10.1	40.4	36.5	40.6
Fe_2O_3 calculated	2.62	1.93	33.9	27.2	37.5	35.7	5.20	10.2	6.65	11.3	44.9	40.6	45.1
MgO	0.03	0.27	0.16	0.21	0.20	0.48	0.45	0.75	0.45	0.74	bdl	0.01	bdl
CaO	12.3	11.3	3.73	2.50	5.24	10.9	1.22	1.36	1.27	1.57	0.08	0.21	0.22
K_2O	bdl	0.03	0.14	0.07	0.15	0.15	0.10	0.04	0.06	0.02	7.20	7.16	7.46
P_2O_5	24.7	32.0	34.6	33.9	40.1	29.0	0.20	0.22	0.06	0.10	1.08	1.09	1.03
SO_3	0.20	0.09	0.04	0.12	0.11	0.13	0.07	0.08	bdl	0.05	31.0	27.4	28.9
Total	73.6	79.7	76.8	76.2	87.7	77.6	92.5	90.1	90.4	91.2	50.5	52.6	50.2
apfu													
Si	0.418	0.329	0.098	0.206	0.059	0.128	2.087	2.199	2.153	2.185	0.002	0.123	0.008
Al	2.745	2.557	0.157	0.285	0.192	0.038	1.653	1.319	1.526	1.309	0.125	0.711	0.066
Fe^{3+}	0.159	0.106	0.783	0.612	0.759	0.865	0.160	0.324	0.209	0.357	0.000	0.000	0.000
Mg	0.004	0.029	0.007	0.009	0.008	0.023	0.028	0.047	0.028	0.047	0.000	0.001	0.000
Ca	1.060	0.880	0.123	0.080	0.151	0.377	0.053	0.062	0.057	0.071	0.008	0.022	0.025
K	0.000	0.003	0.005	0.003	0.005	0.006	0.005	0.002	0.003	0.001	0.893	0.890	0.973
P	1.683	1.969	0.901	0.857	0.913	0.791	0.007	0.008	0.002	0.004	0.089	0.090	0.089
S	0.012	0.005	0.001	0.003	0.002	0.003	0.002	0.003	0.000	0.002	2.263	2.002	2.218
Total cations	6.081	5.878	2.081	2.056	2.094	2.231	3.995	3.964	3.978	3.974	6.722	6.827	6.875
Oxygens	10.50	10.50	4	4	4	4	7	7	7	7	11	11	11

5.6. Mössbauer

The Mössbauer spectra of the three measured samples consist of quadrupolar doublets and magnetic sextets, as shown in Figure 10 (only those of samples 5/7-3.1 and 5/11-2.A2 are given while the refined values of the hyperfine parameters are listed in Table 3). The values of the isomer shift were consistent with the exclusive presence of the Fe^{3+} species (in high-spin state) with no detectable trace of the Fe^{2+} species. The spectra at 300 K and 77 K of sample 5/11-2.A2 (Figure 10b) consisted only of a slightly asymmetrical doublet (Δ~0.5–0.6 mm/s). In contrast, the spectra of samples 11S-N4 and 5-7/3.1 (Figure 10a) can be decomposed in at least two distinct quadrupolar doublets (Δ~0.5–0.6 mm/s and Δ~1.2–1.3 mm/s) with rather similar area ratios (2:1) between the narrow and broad lines' doublets. At low temperatures (77 K), the quadrupolar component with narrow lines remained basically unchanged while that with the broadened lines split into a quadrupolar doublet and a magnetic sextet.

Table 3. Refined values of hyperfine parameters of Mössbauer spectra. Γ (mm/s): full width at half maximum peak; δ_{Fe} (mm/s): isomer shift; Δ (mm/s): quadrupolar splitting; 2ε (mm/s): quadrupolar shift; and B_{hf} (T): hyperfine field.

Sample	T (K)	δ_{Fe} (mm/s) ±0.02	Γ (mm/s) ±0.02	Δ (mm/s) ±0.02	2ε (mm/s) ±0.02	B_{hf} (T) ±0.5	% ±2	Interpretation
11N-L4	300	0.42	0.46	0.45			61	Fe^{3+} (SP * goethite + variscite?)
		0.37	0.33	1.24			39	Fe^{3+} (jarosite?)
	77	0.52	0.53	0.42			54	Fe^{3+} (SP * goethite + variscite?)
		0.47	0.36	1.22			35	Fe^{3+} (jarosite?)
		<0.51>			<−0.23>	<48.3>	11	Fe^{3+} (goethite)
5/7-3.1	300	0.39	0.57	0.60			65	Fe^{3+} (SP * goethite + variscite?)
		0.37	0.28	1.27			35	Fe^{3+} (jarosite?)
	77	0.50	0.64	0.56			43	Fe^{3+} (SP * goethite + variscite?)
		0.48	0.38	1.27		-	33	Fe^{3+} (jarosite?)
		<0.51>			<−0.25>	<48.3>	24	Fe^{3+} (goethite)
5/11-2.A2	300	0.39	0.62	0.48			100	Fe^{3+} (SP * goethite + variscite?)
	77	0.48	0.78	0.50		-	100	Fe^{3+} (SP * goethite + variscite?)

* SP means superparamagnetic.
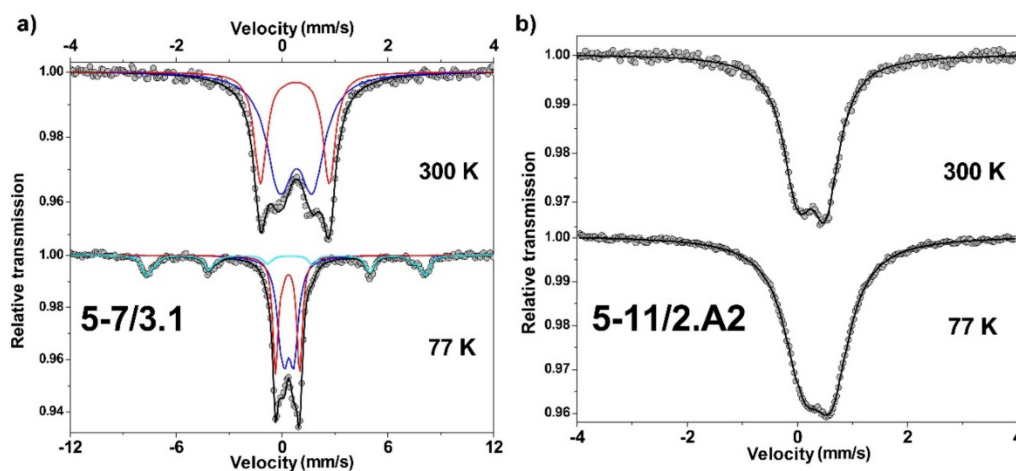
Figure 10. Mössbauer spectra of (**a**) sample 5-7/3.1 and (**b**) sample 5-11/2.A2 recorded at 300 K and 77 K.

According to the values of the hyperfine fit parameters, mainly the negative quadrupolar shift (see Table 3) and the magnetic sextet at 77 K (in samples 11S-N4 and 5-7/3.1) can be easily attributed to goethite (α-FeOOH). Indeed, the hyperfine structure strongly depends on the size of the grains of goethite: when this phase occurs with large grains, the Mössbauer spectra at RT and 77 K consist of a magnetic sextet in agreement with a static magnetic structure ($T_N \sim 399$K). When the size of the grains remains in the range of 10–20 nm, the RT spectrum becomes a quadrupolar doublet as they behave as superparamagnets (SP), while the 77 K spectrum remains as a magnetic sextet, resulting in a blocked magnetic structure. In the presence of ultrafine grains ($<\sim10$–15 nm) of goethite, the RT and 77 K spectra consist of quadrupolar doublets, resulting in the presence of superparamagnetic relaxation phenomena [58]. Therefore, in the present study, the 11S-L4 and 5/7-3.1 samples should contain fine goethite grains while sample 5/11-2.A2 may contain ultrafine goethite grains.

The interpretation of the component with a larger quadrupolar splitting, as observed in samples 11S-L4 and 5/7-3.1, is not straightforward. Variscite formally does not contain iron but both phosphosiderite and its dimorph strengite have similar structures to variscite and their Mössbauer spectra contain two slightly different Fe^{3+} narrow doublets [59,60]. The presence of any of these two iron phosphates (or simply iron-substituted variscite) in the analyzed Gavà samples would contribute to broadening the narrow sextet by overlapping largely with the SP goethite doublet but they cannot be related to the wide doublet. Among the list of possible candidates to explain the wide magnetic doublet, the known hyperfine parameters of jarosite ($KFe(SO_4)_2(OH)_6$ [61]) could match the observed wide Fe^{3+} doublet.

6. Discussion

6.1. Greenish Geological and Archaeological Samples: Mineralogy and Distribution

A reliable determination of the factors that control the variscite colours and their corresponding distribution in the deposit is essential to understand the history of the mining exploitation and the links with the commercial network of variscite during the Neolithic period. There are hundreds of archaeological sites (in Catalonia and abroad) where variscite ornaments have been found, presumably extracted from Gavà [62,63]. Thus, it is necessary to increase the knowledge about the distribution of different styles of samples in the Gavà area. An important question is: could the variscite colour be controlled by the stratigraphic depth? [21] suggested that the strongest green variscite would be associated to the lowest levels of the profile, while pale green and brownish-coloured samples, would be found in the uppermost levels. However, the systematic and extensive sampling carried out in this study, that also included new excavated archaeological sites (e.g., ASA), suggests that this model is not valid. The colour of variscite is not related to the stratigraphic profile depth.

Previous detailed mapping of the GMAP concluded that almost all the mining galleries and pits were carried out to follow veins or beds made up of greenish minerals [20,43–46]. Moreover, the colourimetric study shows that different shades of green are present in the 28 mineral samples of the geological and archaeological origin samples at GMAPThe bulk identification by XRD of ores still remaining in the galleries demonstrates the occurrence of different mineral species, i.e., phosphates (variscite, turquoise, crandallite, phosphosiderite, and montgomeryite), sulphates (jarosite and alunite), and silicates (quartz, halloysite, kaolinite, and smectite). Most of these minerals are found in all the sampled levels of the mine profiles. Some of them, such as kandite, alunite, jarosite, and crandallite, are typical components of oxidizing acid alteration, in this case, connected with the weathering of the sulphides that are disseminated into the black shales; variscite and phosphosiderite, themselves, are minerals typically found in acidic soils [64–66]. Hence, oxidizing acid fluids were able to sink into the bleached black shales and react with them to produce these minerals.

In spite of the spread distribution of all the minerals across the mine, veinlets with sheet silicates of the kandite and smectite groups tend to dominate in the uppermost levels

of the exploitations, being rarer in the deepest ones (Figure 11). However, they are rarely found in archaeological samples. When they occur in archaeological objects, they are mixed with variscite or turquoise in different grades (Table 2). In fact, although the greenish-yellow colour of clay minerals can be very similar to that of variscite, the mechanical properties of clays disable them to be carved for ornaments. Hence, the near-to-surface galleries and pits that follow veinlets of greenish Fe-rich smectite or Fe-rich kaolinite could be simply prospections where greenish sheet-silicates were confused with better-quality variscite veins. In fact, in all of the cases, these galleries were abandoned.
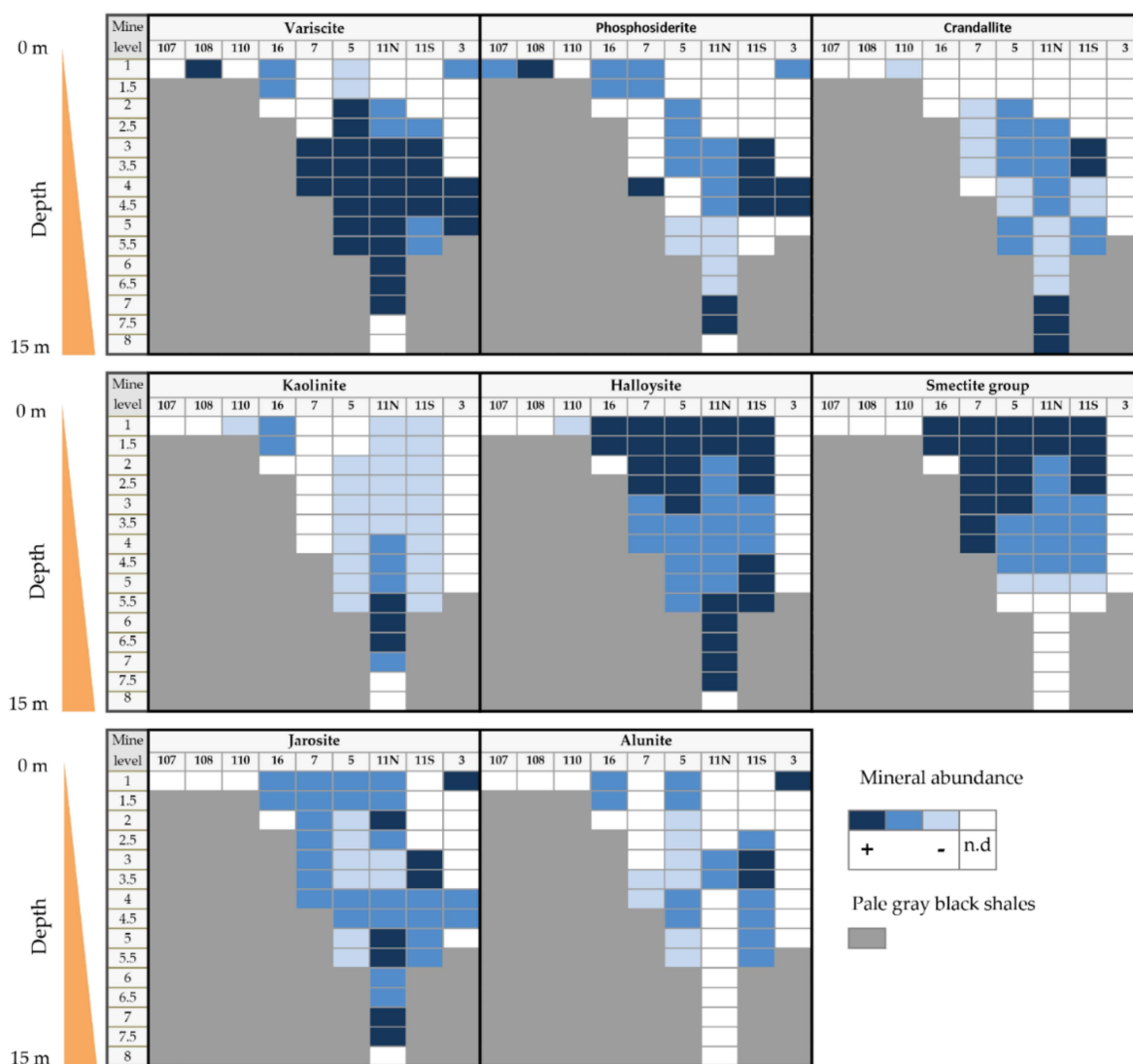

Figure 11. Abundance distribution in depth of the different green-to-brown minerals (variscite, phosphosiderite, crandallite, kaolinite, smectite group, jarosite, and alunite) located in the veins of the GMAP mines.

Turquoise has not been found in any of the studied mines, although it has been found in the archaeological samples found in mine 16. Therefore, the found turquoise beads would have been extracted in another sector, outside our study area. For instance, abundant veins (2–3 cm wide) made up by intimate mixtures of turquoise with crandallite were found in some outcrops nearby to the 20 m N of the GMAP [44].

6.2. Green Colour in Variscite: Influence of the Chemical Composition

Pure variscite samples from Gavà may have different shades of green, with the classical strong green varieties being the most appreciated. The green colour cannot be attributed in these cryptocrystalline varieties to the occurrence of a major chemical component, such as Fe. In fact, the Fe content of single variscite grains has no correlation with the colour of the piece. Other possible chromophore elements in variscite, such as Mn, are absent in the Gavà samples. Moreover, the Mössbauer study of the Gavà variscite discards the simultaneous occurrence of Fe in different stages of the oxidation in the variscite structure (Fe^{2+} and Fe^{3+}), which could be very effective in the generation of colour. All the variscite samples in the Gavà area corresponded to the Messbach type; therefore, the colour cannot be attributed to the change from one polytype to another as described by [28].

The difference in green/blue hues can be roughly attributed to differences in the Cr^{3+} content, as described by [26,28]. The specimens with more intense green colours, such as GM-11N-5.1, GM_11N-L4, or GM-5/7.5.1, are those with a higher content of Cr^{3+} (Table 2 and Figure 12). Oppositely, samples with a very pale green colour, such as GM-7-4.5, corresponded to samples with the lowest Cr^{3+} contents. As a set, the Cr (and V) values in Gavà are low when compared with green variscite from the Palazuelo de las Cuevas mines (in the order of 0.04% Cr_2O_3 [28,67] and regarding other outcrops in the Iberian Peninsula [49,68]). However, these low V and Cr results from Gavà must be used with caution: they are diluted because variscite is intimately mixed with variable amounts of other cryptocrystalline minerals devoid of Cr or V, such as quartz, clay minerals, other phosphates, jarosite, or goethite, as was revealed by the SEM-EDS, EMPA, Raman, and Mössbauer analyses. Therefore, the real proportion of Cr and V in the Gavà variscite samples can be slightly higher.
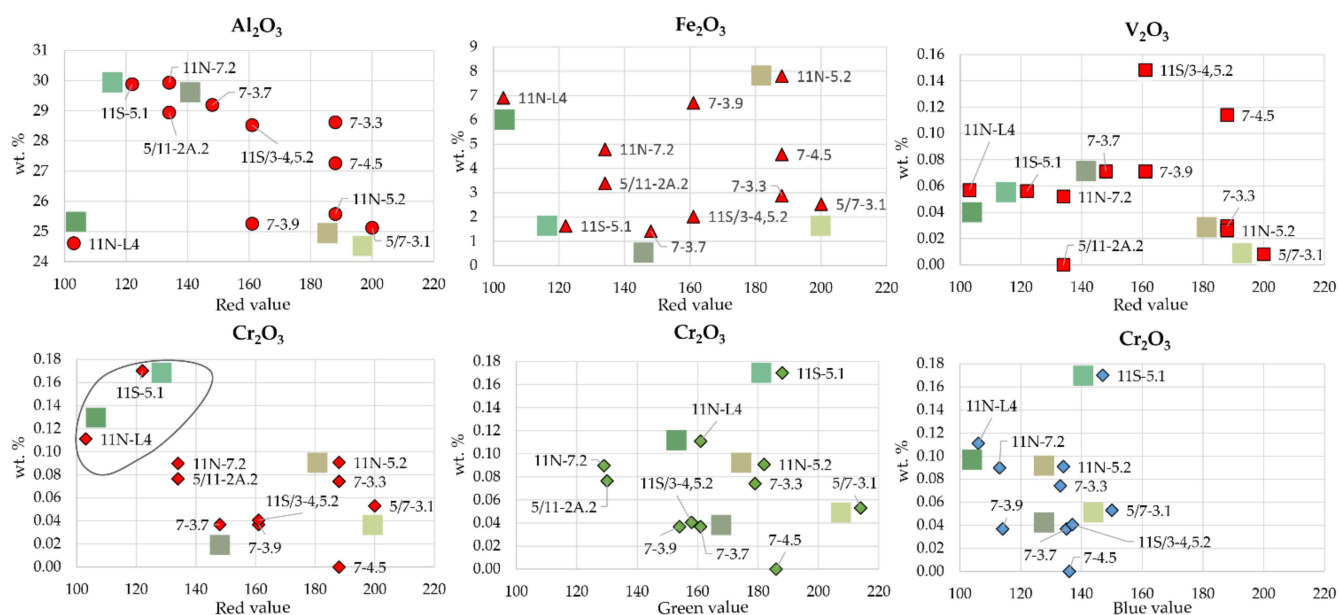
Figure 12. Variscite colour variation related to the content of some relevant elements. Note the anti-correlation between the red value and the predominance of the green value and Cr_2O_3 contents. Different green colour boxes indicate colourimeter results in five representative samples.

6.3. Green Colour in Variscite: Influence of Mineral Mixtures

Variscite, in different shades of green (e.g., samples GM-5/11-2A2, GM-5/5-3.1, or GM-11S-5.1), is very abundant from level 1/2 (−2 to −4 m from the surface) to level 7 (almost −15 m deep). The colour distribution throughout the profile is not uniform and can be olive green, intense mossy green, and whitish green at the same level (Figure 9). The same colours of the mineral variscite described are found in archaeological beads manufactured during the Neolithic period both in the Can Tintorer sector and in those found in the Les

Ferreres sector. In all of these occurrences, cryptocrystalline variscite is intimately mixed with other minerals of different colours, as revealed by the XRD, SEM-EDS, EMPA, and Mössbauer analyses. Hence, the resulting colour of the mixtures will be the sum of the different colours of the respective minerals and will also vary depending on the proportion of each mineral in the mixture.

The phosphosiderite found in Gavà is cryptocrystalline and black, and brown to ochre in colour; hence, intimate mixtures with variscite cause most of the brownish hues in variscite (e.g., sample GM-16.4). A similar issue arises with jarosite–variscite mixtures (e.g., sample GM-3/11-4,5.2). On the other hand, Mössbauer data revealed that in at least a part of the variscite samples, contents of Fe^{3+} obtained in the EMPA analyses can be the result of the occurrence of traces of microcrystalline goethite and possibly jarosite (both can contribute, adding, occasionally, an ochre hue to the samples).

Alunite, halloysite, and crandallite, however, are frequently colourless or milky when pure, but ochre when they are intimately mixed with goethite. When associated with variscite, these minerals may occur as discrete bands or patches (e.g., GM-ASA-1). However, detailed examination of the samples with SEM-BSE-EDS revealed the systematic occurrence of intimate mixtures at the cryptocrystalline scale involving these phosphates, silicates, sulphates, and oxides. Hence, in all these cases, the mixture colour is the combination result of the corresponding minerals' colour. The resulting colouration depends on colours of the different minerals and their respective proportions (Figure 13).
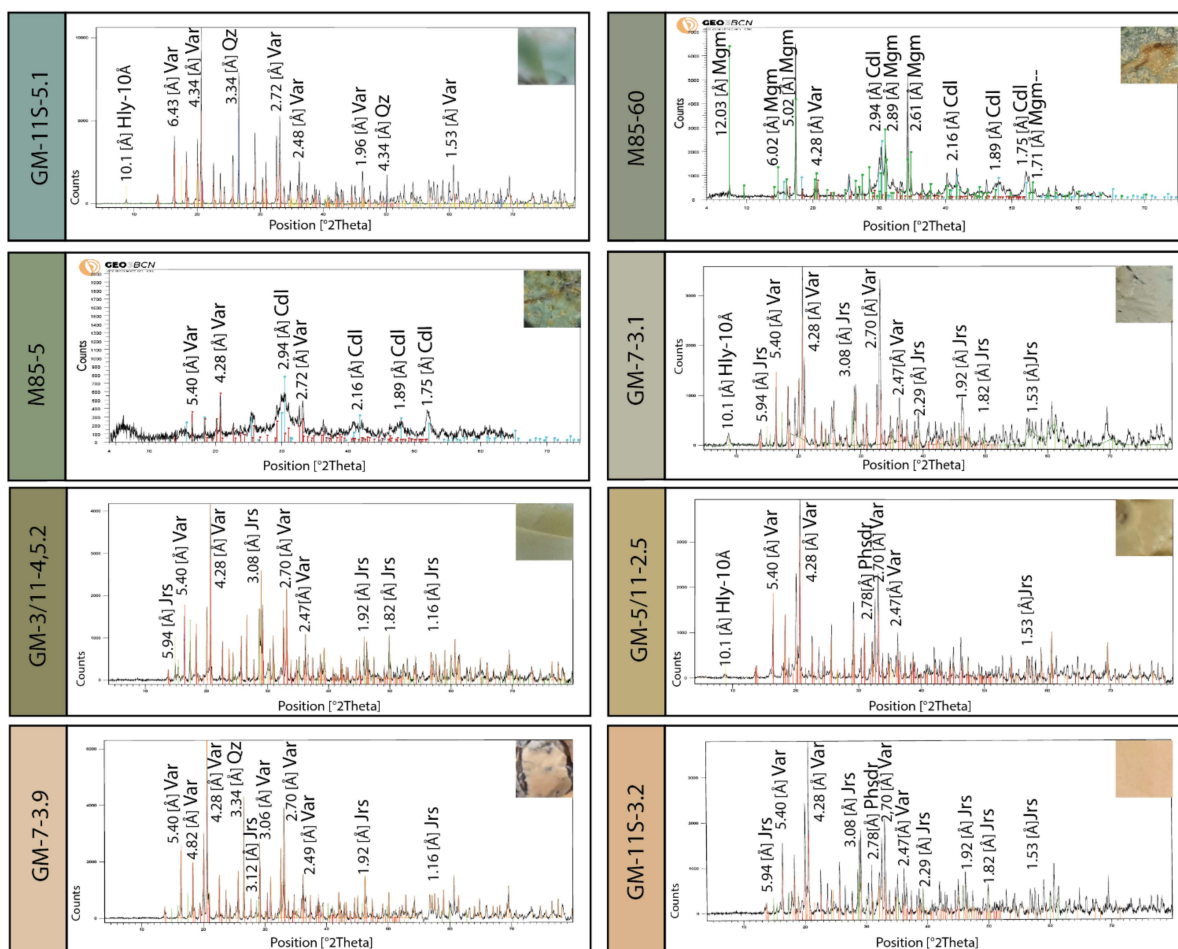
Figure 13. Selected X-ray powder diffractograms representative of variscite mixtures with different mineral associations and the corresponding colour that results. The most characteristic reflections of the dominant minerals have been indicated. Legend: Var, variscite; Hly-10Å, halloysite 10Å; Qz, quartz; Mgm, montgomeryte; Cdl, crandallite; Phsd, phosphosiderite; and Jrs, jarosite.

Similar conclusions related to the role of mixtures on the variscite colour were obtained by [69] when studying the Raman spectra of gemmy green variscite currently exploited for ornaments in different worldwide mines. These authors did not observe significant variations in the Raman spectra but if the colour changed to paler shades, it could be explained by mixtures with the spectra of other minerals. Hence, most of variscite in Gavà is mixed with other minerals in different grades and this can generate large variations in both green hues and apparent low Cr^{3+} contents. Finally, as indicated, the Fe^{3+} content in variscite is probably related to tiny intergrowths with phosphosiderite, jarosite, goethite, and perhaps other Fe^{3+}-rich minerals at least in the Gavà case. Thus, Cr^{3+} contents are not probably significant enough to distinguish provenances, as suggested by [70], and should be taken with caution and only when Fe^{3+} is reliably found into the variscite structure.

Colour into the original veins can vary suddenly or progressively. The latter is the most common case because of the existence of metasomatic replacement fronts and veining of the early formed cryptocrystalline as well as porous minerals by successive pulses of late fluids. As a consequence, the colour varies progressively across the veins and nodules. A nice example is provided in the nodule of sample GM-ASA-1 (Figure 3); details of the thin section reveal progressive changes in the colour from the gray crandallite core to a pale green unit made up by crandallite-dominant mixtures with variscite and finally to deep green variscite-dominant rims (Figure 14).
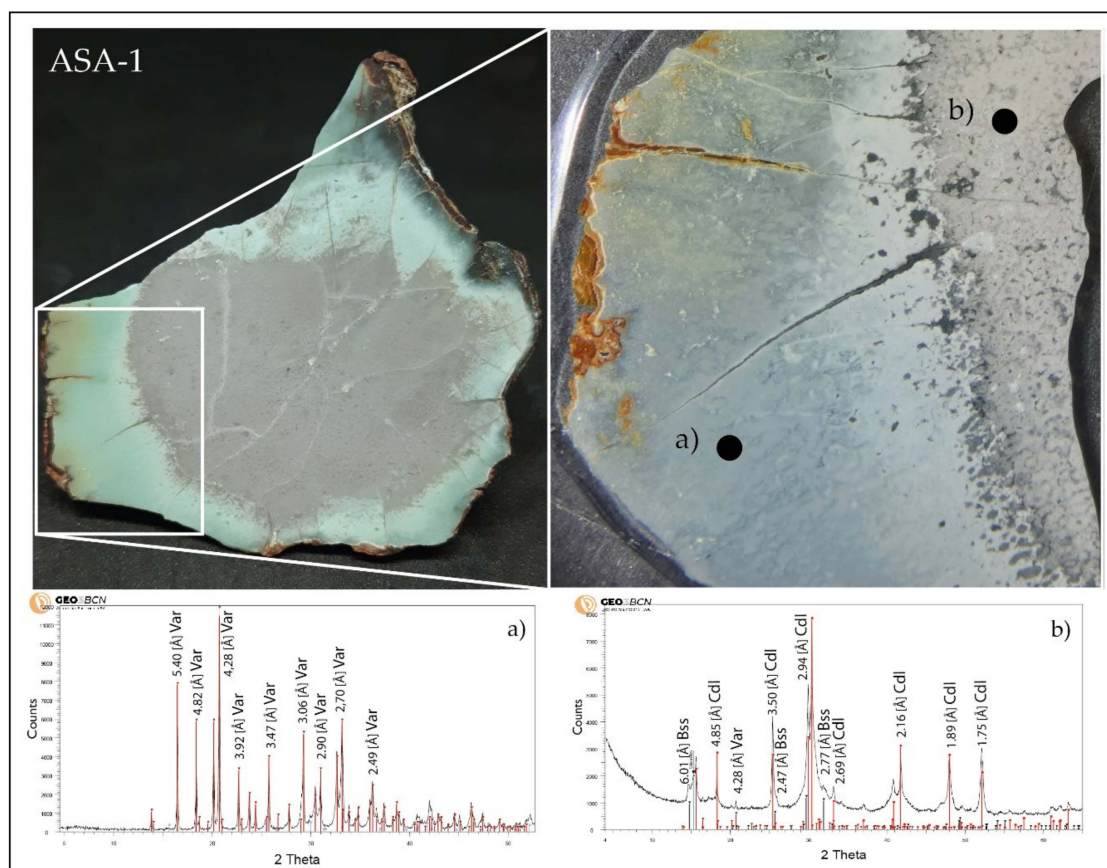

Figure 14. Nodule with a crandallite core (gray) and a variscite rim (green); the right image is a detail of the above. The position of the corresponding XRD scans is indicated on the detailed images. Note the progressive replacement of crandallite by variscite and the existence of an intermediate zone of very pale green material near the contact between both units, which corresponds to an area with crandallite–variscite mixtures dominated by crandallite. Legend: Var, variscite; Cdl, crandallite; and Bss, bassanite. (**a**) variscite x-ray powder diffractogram; (**b**) crandallite, variscite, bassanite x-ray powder diffractogram.

This study reveals that, indeed, during the Neolithic period, the mineral used for necklace beads was selectively chosen according to their colour and properties. Archaeological samples are mostly made up by pure variscite and turquoise but sometimes they can present impurities of other minerals such as halloysite, crandallite, or phosphosiderite.

6.4. Variscite Vs. Turquoise by Colour

The results of the colourimetry combined with samples' mineral characterization clearly mark two groups with two different trends (Figure 15). The variscite samples, including both mineral and archaeological samples, follow an upward linear trend that goes from 120 to 220 in the green value and from 90 to 180 in the blue value. The archaeological samples of turquoise generally show values of green between 200 and 240 and of blue between 180 and 200. Only one case of the turquoise sample (M16-1511) does not follow this trend, as seen in Figure 4. In this particular sample, the turquoise colour is masked by a yellowish patina and this explains the different chromatic behavior.
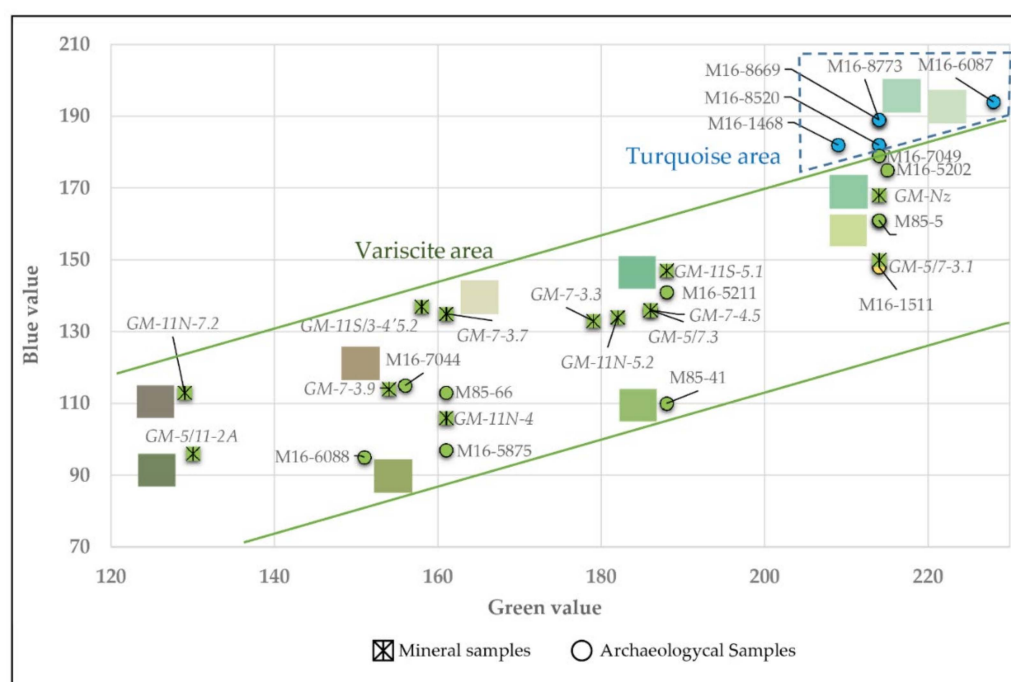
Figure 15. Representation of colourimetry results with their mineral characterization: five samples characterized as turquoise (in blue) and 22 samples characterized as variscite (in green).Yellow corresponds to the turquoise with a patina (one sample). Mineral samples are represented with an asterisk and archaeological samples with circles.

The colourimeter appears as a quick and useful tool to differentiate, by colour, variscite from turquoise in the Gavà area as long as they present the colour in the purest possible condition.

7. Conclusions

1. Neolithic galleries and pits of the Gavà mines follow pure variscite veins but also veins with variscite mixtures with other phosphates (e.g., turquoise, phosphosiderite, montgomeryite, or crandallite), sulphates (alunite and jarosite), or silicates (kaolinite, halloysite, quartz, and smectite). Mining operations opened to exploit veins with pure green clays are rare and were abandoned only a few meters from the mine entrance.
2. Archaeological samples are composed of variscite and turquoise. This fact, along with the scarce length of the excavations that follow pure clay veins, suggests that some galleries were opened as prospective works. Fe-rich smectite can be easily confused

with variscite according to their similar colour but these kinds of silicates are not suitable for the manufacturing of ornaments.

3. The green colour of variscite seems to be correlated with Cr^{3+} enrichment. Despite the low Cr^{3+} contents of the Gavà variscite (compared to other similar mineralizations), samples with more Cr^{3+} also correspond to those with a more intense colour.

4. If variscite is intimately mixed with other cryptocrystalline white minerals (e.g., crandallite, alunite, quartz, or kaolinite), the resulting green colour is paler. If variscite is mixed with goethite, jarosite, or phosphosiderite, then it tends to acquire a yellowish hue. Therefore, gemmy variscite requires high contents of Cr^{3+} and a low proportion of a mixture with other minerals, particularly yellow-brownish minerals.

5. Up to the present moment, turquoise has not been found in the excavated Gavà mines. However, it has been identified in five archaeological specimens from mine 16 of the GMAP. It is reasonable to assume that this turquoise was extracted from hidden or unexcavated Gavà mines but other hypotheses, such as the importation of turquoise from other localities, cannot be ruled out.

6. The colourimeter has proven to be an efficient tool to easily differentiate turquoise and variscite from the Gavà area provided that the mineral does not present surface patinas that could disrupt the original colour.

References

1. Nassau, K. The origins of colour in minerals. *Am. Mineral.* **1978**, *63*, 219–229.
2. Burns, R. *Mineralogical Applications of Crystal Field Theory. Cambridge Topics in Mineral Physics and Chemistry*, 2nd ed.; Cambridge University Press: Cambridge, UK, 1993; p. 480.
3. Mattson, S.M.; Rossman, G.R. Identifying characteristics of charge transfer transitions in minerals. *Phys. Chem. Miner.* **1987**, *14*, 94–99. [CrossRef]
4. Bill, H.; Calas, G. Colour centers, associated rare-earth ions and the origin of colouration in natural fluorites. *Phys. Chem. Miner.* **1978**, *3*, 117–131. [CrossRef]
5. Krambrock, K.; Ribeiro, L.; Pinheiro, M.; Leal, A.S.; Menezes, M.A.; Spaeth, J. Colour centers in topaz: Comparison between neutron and gamma irradiation. *Phys. Chem. Miner.* **2007**, *34*, 437–444. [CrossRef]
6. Lindberg, M.L.; Pecora, W.T. Phosphate minerals from Sapucaia Pegmatite Mine, Minas Gerais. *Bol. Soc. Bras. Geol.* **1958**, *7*, 5–14.
7. Cassedanne, J.P.; Baptista, A. Famous mineral localities: The Sapucaia pegmatite, Minas Gerais, Brazil. *Mineral. Rec.* **1999**, *30*, 347–360.
8. Segnit, E.R.; Francis, G.L. Secondary phosphate minerals from Iron Monarch, South Australia. *Aust. Mineral.* **1983**, *43*, 243–250.

9.   Barwood, H. Red and Pink Variscite from the Wood Mine, Cocke County, Tennessee. *Rocks Miner.* **1997**, *72*, 268–270. [CrossRef]
10.   Meireles, C.; Ferreira, N.; Lourdes, R.M. Variscite Occurrences in Silurian Formations from Northern Portugal. *Comun. Dos Serviços Geológicos De Port.* **1987**, *73*, 21–27.
11.   Herbaut, F.; Querré, G. La parure néolithique en variscite dans le sud de l'Armorique. *Bull. Société Préhistorique Française* **2004**, *101*, 497–520. [CrossRef]
12.   Fernández Turiel, J.L.; Blanco Majado, J.; López Alonso, M.; Edo, M. Estudio analítico de determinación mineralógica y de composición química de las cuentas de collar de calíta y otras materias primas del yacimiento de Las Peñas (Quiruelas de Vidriales, Zamora). *Rubricatum* **1995**, *1*, 227–237.
13.   Odriozola, C.P.; Linares-Catela, J.A.; Hurtado Pérez, V. Variscite source and source analysis: Testing assumptions at Pico Centeno (Encinasola, Spain). *J. Archaeol. Sci.* **2010**, *37*, 3146–3157. [CrossRef]
14.   Odriozola, C.P.; Linares-Catela, J.A.; Hurtado-Pérez, V.M. Provenancing variscite beads: Pico Centeno (Encinasola, Spain) outcrop case study. *Open J. Archaeom.* **2013**, *1*, 80–84. [CrossRef]
15.   Villalobos, R.; Odriozola, C.P. Organizing the production of variscite personal ornaments in later Prehistoric Iberia: The mines of aliste and the production sites of Quiruelas de Vidriales (Zamora, Spain). *Eur. J. Archaeol.* **2016**, *19*, 631–651.
16.   Acevedo, N.; Weber, M.; García-Casco, A.; Proenza, J.A.; Sáenz, J.; Cardona, A. A first report of variscite Tairona (A.D. 1100–1600) from the Sierra Nevada de Santa Marta, Colombia, and its implications for Precolumbian exchange networks in the region. *Lat. Am. Antiq.* **2007**, *27*, 549–560. [CrossRef]
17.   Acevedo, N.; Weber, M.; Proenza, J.A.; García-Casco, A.; Sáenz-Samper, J. Provenance study of the variscite artifacts of the Sierra Nevada de Santa Marta, Colombia and approach to routes of pre-Hispanic exchange. *J. Archaeol. Sci.* **2021**, *136*, 105511. [CrossRef]
18.   Ball, S.H. *The Mining of Gems and Ornamental Stones by American Indians*; Bureau of American Ethnology Bulletin 128, Anthropological Papers 13; Smithsonian Institution: Washington, DC, USA, 1941; p. 77.
19.   Willing, M.; Stocklmayer, S.; Wells, M. Ornamental variscite: A new gemstone resource from Western Australia. *J. Gemmol.* **2008**, *31*, 111–124. [CrossRef]
20.   Díaz-Acha, Y.; Campeny, M.; Tauler, E.; Bosch, J.; Melgarejo, J.C.; Camprubí, A.; Villanova-de-Benavent, C.; Jorge-Villar, S.; Díaz-Ontiveros, I.; Fernández-Lluch, D.; et al. Critical Elements in Supergene Phosphates: The Example of the Weathering Profile at the Gavà Neolithic Mines, Catalonia, Spain. *Minerals* **2020**, *10*, 3. [CrossRef]
21.   Melgarejo, J.C.; Arqués, L.; Villanova-de-Benavent, C.; Jahwari, T.; Torró, L.; Bosch, J.; Castillo-Oliver, M.; Campeny, M.; Amores, S.; Andreazini, A.; et al. The use of Raman spectroscopy in the characterization of variscite provenance: The Gavà case. In *La Parure en Callaïs du Néolithique Européen*; Archaeopress: Oxford, UK, 2019; pp. 241–251.
22.   Fritsch, E.; Rossman, G.R. An update on colour in gems. Part 1: Introduction and colours caused by dispersed metal ions. *Gemst. Gemol.* **1987**, *23*, 126–139. [CrossRef]
23.   Foster, M.D.; Schaller, W.T. Cause of colour in wavellite from Dug Hill, Arkansas. *Am. Mineral.* **1996**, *51*, 422–428.
24.   Marty, J.; Howard, D.G.; Barwood, H. *Minerals of the Utahlite Claim, Lucin, Box Elder County, Utah*; Utah Geological Survey Miscellaneous Publication: Salt Lake City, UT, USA, 1999; p. 16.
25.   Rossman, G.R. *Mineral Spectroscopy Server*; California Institute of Technology: Pasadena, CA, USA, 2004; Available online: http://minerals.gps.caltech.edu/FILES/Visible/Variscite/Index.html (accessed on 15 March 2022).
26.   Calas, G.; Galoisy, L.; Kiratisin, A. The origin of the green colour of variscite. *Am. Miner.* **2005**, *90*, 984–990. [CrossRef]
27.   Salvador, P.; Fayos, J. Some aspects of the structural relationship between "Messbach-type" and "Lucin-type" variscites. *Am. Miner.* **1972**, *57*, 36–44.
28.   García-Guinea, J.; Correcher, V.; Sánchez Muñoz, L.; López-Arce, P.; Townsend, P.; Hole, D. Radiation damage of variscite in historic crafts: Solarization, decolouration, structural changes and spectra from ionoluminescence. *Radiat. Phys. Chem.* **2008**, *77*, 18–22. [CrossRef]
29.   Alonso, M.; Edo, M.; Gordo, L.; Millán, M.; Villalba, M.J. Explotación minera neolítica en Can Tintoré (Gavà, Barcelona). *Pyrenae* **1978**, *13*, 7–14.
30.   Villalba, M.J.; Blasco, A.; Edo, M.; Bañolas, L.; Arenas, J. Minería neolítica: Can Tintorer, una aportación fundamental. *Rev. Arqueol.* **1989**, *96*, 13–24.
31.   Villalba, M.J.; Bañolas, L.; Arenas, J. Can Tintorer (Gavà, Catalunya): Une exploitation néolithique de phosphates et silicates. *Cah. Du Quat.* **1990**, *17*, 275–285.
32.   Villalba, M.J. Le gîte de variscite de Can Tintorer: Production, transformation, et circulation du minéral vert. In *Matériaux, Productions, Circulations du Néolithique à l'âge du Bronze: Paris, France*; Guilaine, J., Ed.; Éditions Errance: Paris, France, 2002; pp. 115–129.
33.   Blasco, A.; Edo, M.; Villalba, M.J. *Les Perles en Callaïs du Sud de la France: Proviennent-Elles des Mines de Can Tintorer? Montpellier, France, Conseil Général de l'Hérault, Le Chalcolithique en Languedoc, Ses Relations Extra-Régionales (Saint Mathieu de Tréviers, 1990), Archéologie en Languedoc*; Colloque International Hommage au Dr. Jean Arnal: Saint Mathieu de Tréviers, France, 1991; pp. 279–289. Available online: https://www.researchgate.net/publication/292140097_Les_perles_en_callais_du_Sud_de_la_France_proviennent-elles_des_Mines_de_Can_Tintorer (accessed on 15 March 2022).
34.   Blasco, A.; Villalba, M.J.; Edo, M. Cronologia del complex miner de Can Tintorer. Aportacions a la periodització del Neolític mitjà català: Puigcerdà, Catalonia, 9è Col·loqui Internacional d'Arqueologia de Puigcerdà. In *Estat de la Investigació Sobre el Neolític a Catalunya*; Institut d'Estudis Ceretans: Barcelona, Spain, 1992; pp. 215–219.

35. Blasco, M.; Borrell, M.; Bosch, J. Las minas prehistóricas de Gavà (Barcelona): Un ejemplo de estudio, conservación y presentación pública de un yacimiento arqueológico. *Trab. Prehist.* **2000**, *57*, 77–87. [CrossRef]

36. Bosch, J.; Estrada, A.; Noain, M.J. Minería neolítica en Gavá (Baix Llobregat, Barcelona). *Trab. Prehist.* **1996**, *53*, 59–71. [CrossRef]

37. Bosch, J.; Gómez, A. Estudi de les ceràmiques neolítiques procedents de les mines 83, 84, 85 i 90 de Gavà. *Rubricatum* **2009**, *4*, 63–83.

38. Borrell, F.; Estrada, A. Elements ornamentals neolítics de variscita trobats a les mines 83 i 85 de Gavà. *Rubricatum* **2009**, *4.*, 171–181.

39. Borrell, F.; Orri, E. Excavacions arqueològiques a la serra de les Ferreres, Mines Prehistòriques de Gavà. In *L'Arqueologia a Gavà. Homenatge a Alícia Estrada: Gavà, Catalonia, Ajuntament de Gavà/Amics del Museu de Gavà, Collecció La Nostra Gent*; Museu de Gavà: Gavà, Spain, 2009; pp. 67–86. Available online: https://www.researchgate.net/publication/305073009_Excavacions_ arqueologiques_a_la_serra_de_les_Ferreres_Mines_Prehistoriques_de_Gava (accessed on 15 March 2022).

40. Borrell, F.; Bosch, J. Las minas de variscita de Gavà (Barcelona) y las redes de circulación en el Neolítico. *Rubricatum* **2012**, *5*, 315–322.

41. Borrell, F.; Bosch, J.; Majó, T. Life and death in the Neolithic Variscite Mines at Gavà (Barcelona, Spain). *Antiquity* **2015**, *89*, 72–90. [CrossRef]

42. Borrell, F.; Bosch, J.; Gibaja, J.F.; Schmidt, P.; Terradas, X. The status of imported Barremian-Bedoulian flint in north-eastern Iberia during the Middle Neolithic. Insights from the variscite mines of Gavà (Barcelona). *PLoS ONE* **2019**, *14*, 1–29. [CrossRef]

43. Costa, F.; Camprubí, A.; Melgarejo, J.C. Aproximación geológica a las minas neolíticas de fosfatos férrico-alumínicos de Gavà (Cataluña). *Bol. Geol. Min.* **1994**, *105*, 436–443.

44. Camprubí, A.; Melgarejo, J.C.; Proenza, J.A.; Costa, F.; Bosch, J.; Estrada, A.; Borrell, F.; Yushkin, N.P.; Andreichev, V.L. Mining and geological knowledge during the Neolithic: A geological study on the variscite mines at Gavà, Catalonia. *Episodes* **2003**, *26*, 295–301. [CrossRef] [PubMed]

45. Díaz-Acha, Y.; Melgarejo, J.C.; Bosch, J.; Andreazini, A.; Pastor, M.; Pujol-Solà, N.; Campeny, M.; Torró, L.; Villanova-de-Benavent, C.; Castillo-Oliver, M.; et al. The Neolithic variscite mines of Gavà, Catalonia: Criteria for mineral exploration and exploitation in the Prehistory. *Bol. Soc. Geol. Mex.* **2019**, *71*, 83–319. [CrossRef]

46. Díaz-Acha, Y.; Campeny, M.; Melgarejo, J.C.; Bosch, J.; Lehbib, S.; Torró, L.; Proenza, J.A.; Castillo-Oliver, M.; Camprubí, A.; Villanova-de-Benavent, C.; et al. Geological context of the historic and prehistoric iron mines in the Gavà area, Catalonia, NE Iberian peninsula. *Bol. Soc. Geol. Mex.* **2019**, *71*, 321–342. [CrossRef]

47. Noain, M.J. Las cuentas de collar en variscita de las minas prehistóricas de Gavà (Can Tintorer): Bases para un estudio experimental. *Cuad. Prehist. Arqueol.* **1996**, *23*, 37–86.

48. Alarashi, H.; Borrell, F. Constructing identities in Neolithic times. The variscite ornaments of Gavà (Barcelona). In *L'Art du Paraître: Apparences de l'Humain, de la Préhistoire à Nos Jours. The art of Human Appearance, from Prehistory to the Present Day. 40e Rencontres Internationales d'Archéologie et d'Histoire de Nice Côte d'Azur*; Éditions APDCA-CEPAM: Nice, France, 2020; pp. 109–125. Available online: https://www.researchgate.net/publication/345805488_Constructing_identities_in_Neolithic_times_The_ variscite_ornaments_of_Gava_Barcelona_In_book_L%27ART_DU_PARAITRE_APPARENCES_DE_L%27HUMAIN_DE_LA_ PREHISTOIRE_A_NOS_JOURS_THE_ART_OF_HUMAN_APPEARANCE_FROM_PRE (accessed on 15 March 2022).

49. Fernández, A.; Moro, C.; Dabard, M.P. *Les Minéralisations De Variscite Du Sud-Ouest De l'Europe: Caractéristiques Minéralogiques, Géochimiques Et Genèse. La Parure En Callaïs Du Néolithique Européen*; Archaeopress Publishing: Oxford, UK, 2019; pp. 9–23.

50. Anadón, P.; Colombo, F.; Esteban, M.; Marzo, M.; Robles, S.; Santanach, P.; Solé Sugrañés, L. Evolución tectonoestratigráfica de los Catalánides. *Acta Geol. Hisp.* **1979**, *14*, 242–270.

51. Guimerà, J. Palaeogene evolution of deformation in the north-eastern Iberian peninsula. *Geol. Mag.* **1984**, *121*, 413–420. [CrossRef]

52. Santanach, P.; Casas, J.M.; Gratacós, O.; Liesa, M.; Muñoz, J.A.; Sàbat, F. Variscan and Alpine structure of the hills of Barcelona: Geology in an urban area. *J. Ib. Geol.* **2011**, *37*, 121–136.

53. Julivert, M.; Duran, H. Paleozoic stratigraphy of the Central and Northern part of the Catalonian Coastal Ranges (NE Spain). *Acta Geol. Hisp.* **1990**, *25*, 3–12.

54. Julivert, M.; Duran, H.; Rickards, R.B.; Chapman, A.J. Siluro-Devonian graptolite stratigraphy of the Catalonian Coastal Ranges. *Acta Geol. Hisp.* **1985**, *20*, 199–207.

55. Bordas, A.; Borrell, F.; Bosch, J. 10 anys de recerques arqueològiques a la serra de Les Ferreres (mines de Gavà, Baix Llobregat). De la variscita al ferro: Neolític i Antiguitat. *Rubricatum* **2009**, *4*, 10–14.

56. Frost, R.L.; Weier, M.L.; Erickson, K.L.; Carmody, O.; Mills, S.J. Raman spectroscopy of phosphates of the variscite mineral group. *J. Raman Spectrosc.* **2004**, *35*, 1047–1055. [CrossRef]

57. Fritsch, E.; Karampelas, S.; Mevellec, J.Y. Raman spectra of gem-quality variscite and metavariscite. *J. Raman Spectrosc.* **2017**, *48*, 1554–1558. [CrossRef]

58. Brok, E.; Frandsen, C.; Madsen, D.E.; Jacobsen, H.; Birk, J.O.; Lefmann, K.; Bendix, J.; Pedersen, K.S.; Boothroyd, C.B.; Berhe, A.A.; et al. Magnetic properties of ultra-small goethite nanoparticles. *J. Phys. D Appl. Phys.* **2014**, *47*, 365003. [CrossRef]

59. Dyar, M.; Jawin, E.; Breves, E.; Marchand, G.; Nelms, M.; Lane, M.; Mertzman, S.; Bish, D.; Bishop, J. Mössbauer parameters of iron in Phosphate minerals: Implications for interpretation of Martian data. *Am. Mineral.* **2014**, *99*, 914–942. [CrossRef]

60. Balatskiy, D.; Dedushenko, S.; Gritsenko, Y.; Ksenofontov, D.; Perfiliev, Y. X-ray and Mössbauer study of phosphosiderite from Atacama, Chile. *Hyperfine Interact.* **2021**, *242*, 14. [CrossRef]

61. Kovács, K.; Kuzmann, E.; Homonnay, Z.; Vértes, A.; Gunneriusson, L.; Sandström, Å. Mössbauer study of synthetic jarosites. *ICAME* **2009**, *186*, 69–73.

62. Bosch, J. Gavà (Barcelone), mine et atelier au Néolithique. In *La Parure en Callaïs du Néolithique Européen*; Querré, G., Cassen, S., Vigier, E., Eds.; Archaeopress Publishing Ltd.: Oxford, UK, 2019; pp. 43–58.

63. Molist, M.; Oliva, M. La parure en variscite au Néolithique dans la partie est de l'Espagne. In *La Parure en Callaïs du Néolithique Européen*; Querré, G., Cassen, S., Vigier, E., Eds.; Archaeopress Publishing Ltd.: Oxford, UK, 2019; pp. 351–364.

64. Nriagu, J.O.; Moore, P.B. *Phosphate Minerals*; Springer: Berlin, Germany, 1984; p. 442.

65. Prietzel, J. Mobilization of X-ray amorphous and crystalline aluminum and iron phosphates by common soil extraction procedures. *J. Soil Nutr. Soil Sci.* **2017**, *180*, 14–17. [CrossRef]

66. Werner, F.; Mueller, C.W.; Thieme, J.; Gianoncelli, A.; Rivard, C.; Höschen, C.; Prietzel, J. Micro-scale heterogeneity of soil phosphorus depends on soil substrate and depth. *Nat. Comm. Sci. Rep.* **2017**, *7*, 3203. [CrossRef] [PubMed]

67. Fábregas, R.; Rodríguez-Rellán, C. Palazuelo de las Cuevas and the exploitation of variscite in the North-West of Iberia. In *La Parure en Callaïs du Néolithique Européen*; Querré, G., Cassen, S., Vigier, E., Eds.; Archaeopress Publishing Ltd.: Oxford, UK, 2019; pp. 59–70.

68. Domínguez-Bella, S.; Ramos-Muñoz, J. Pico Centeno prehistoric variscite mines (Encinasola, Huelva, SW Spain). In *La Parure en Callaïs du Néolithique Européen*; Querré, G., Cassen, S., Vigier, E., Eds.; Archaeopress Publishing Ltd.: Oxford, UK, 2019; pp. 71–83.

69. Fritsch, E.; Rondeau, B.; Lulzac, Y.; Mocquet, B. Gemmology of gem phosphates: A review with particular attention to variscite. In *La Parure en Callaïs du Néolithique Européen*; Querré, G., Cassen, S., Vigier, E., Eds.; Archaeopress Publishing Ltd.: Oxford, UK, 2019; pp. 25–40.

70. Querré, G.; Calligaro, T.; Cassen, S.; Dabard, M.P.; Domínguez-Bella, S. Provenance des parures en variscite du Néolithique européen: Élaboration d'un modèle chimiométrique. In *La Parure en Callaïs du Néolithique Européen*; Querré, G., Cassen, S., Vigier, E., Eds.; Archaeopress Publishing Ltd.: Oxford, UK, 2019; pp. 105–128.